Onset and demise of coral reefs, relationship with regional ocean circulation on the Wyville Thomson Ridge

Mary Elliot, Christophe Colin, Mélanie Douarin, Edwige Pons-Branchu, Nadine Tisnerat-Laborde, Frédéric Schmidt, Elisabeth Michel, Quentin Dubois-Dauphin, Arnaud Dapoigny, Lorna Foliot, et al.

Onset and demise of coral reefs, relationship with regional ocean circulation on the Wyville Thomson Ridge

Authors : Mary Elliot[1*], Christophe Colin[2], Mélanie Douarin[1], Edwige Pons-Branchu[3], Nadine Tisnérat-Laborde[3], Frédéric Schmidt[2], Elisabeth Michel[3], Quentin Dubois-Dauphin[2], Arnaud Dapoigny[3], Lorna Foliot[3], Serge Miska[2], François Thil[3], Dave Long[4], Eric Douville[3]

1 Laboratoire de Planétologie/Géodynamique, UMR-CNRS 6112, Université de Nantes, Nantes, France.

2 Laboratoire GEOsciences Paris-Sud (GEOPS), Univ. Paris-Sud, CNRS, Université Paris-Saclay, Rue du Belvédère, Bât. 504, 91405 Orsay, France.

3 Laboratoire des Sciences du Climat et de l'Environnement, LSCE/IPSL, CEA-CNRS-UVSQ, Université Paris-Saclay, F-91191 Gif-sur-Yvette, France.

4 British Geological Survey, Currie EH14 4AP, Edinburgh, United Kingdom

* Corresponding author: mary.elliot@univ-nantes.fr

Abstract : Results from a vibrocore collected on the northern edge of the Scottish continental shelf at around 300 m water depth, on the Wyville Thomson Ridge, enable to reconstruct the history of cold water coral (CWC) reef growth and demise during the Holocene period. We report on significant age differences between U/Th and ^{14}C dates obtained on pristine well-preserved CWC (*Lophelia* *pertusa*), which may reflect an diagenetic process that standard quality tests have failed to highlight. Additional ^{14}C dates derived from bivalve fragments (*Venus* sp.) and foraminifera (*Cibicides refulgens*) samples show a gradual ageing with core depth but with significant age inversions in the lower section of the sediment core, which we consider reflects sedimentary mixing. We thus chose to derive an independent age model using planktonic foraminifera *Globigerina bulloides* stable isotope profiles. The vibrocore record is divided into 3 phases: 1- Mixed sediment deposits of glacial age corresponding to the base of the core with ages older than 13 cal ka BP, 2- The end of the deglacial/early Holocene between 13-9 cal ka BP and 3- Finally, the Holocene period from around 9 cal ka BP with abundant *Lophelia pertusa* fossils. Siliciclastic grain size and clay mineralogical composition show two significant shifts at around 13 and 9 cal ka BP indicating changes in sedimentary sources and transport associated with the dynamics and flow patterns of surface currents during the deglaciation and Holocene. Our results show that the onset of CWC reef growth on the Wyville Thomson Ridge occurred around 9 cal ka BP and was associated with a shift in flow patterns of surface currents in this area. This change of circulation patterns induced favourable sedimentological and hydrological conditions for corals to grow, and is associated with large scale modifications of North Atlantic circulation patterns at the end of the deglaciation.

Introduction

A number of environmental factors such as temperature, salinity, density, oxygen availability, carbonate chemistry, food and nutrients and current velocity appear to control coral reef growth in tropical shallow-water zooxanthellate coral reefs (e.g. Veron, 1993; Dullo et al., 2008). However, the specific factors that control growth and settlement of non-zooxanthellate cold water coral (CWC) reefs have yet to be fully understood (Dorschel et al., 2007; White, 2007). These ecosystems were more recently discovered along the NW European continental margin (Dons, 1944; Le Danois, 1948; Teichert et al., 1958, Henriet et al., 1998). Over the past decades of exploration it has become clear that CWC have a world-wide distribution and *Lophelia pertusa* is one of the most common and widespread of the reef framework-forming cold-water corals (Roberts et al., 2006; 2009; Freiwald et al., 2004; 2017). These CWC ecosystems play a key role in marine biodiversity as they provide habitats for many other species. CWC ecosystems occur over a wide range of depth and within a specific range of temperature, salinity, density and physico-chemical conditions (Davies et al., 2008; Findlay et al., 2014; Robinson et al., 2014).

In the North-East Atlantic, CWC predominantly occur along the European continental margin, between ~100 and 1000 m water depth (Freiwald et al., 2004; 2017; Frank et al., 2011; Findlay et al., 2014; Dullo et al., 2008). Several environmental parameters are thought to be important for CWC reef growth in the

NE Atlantic. Seawater temperatures commonly range from 4 to 12°C, density is in the range of 27.35 to 27.65 kg m-3 (Dullo et al., 2008), and near bottom flow dynamics are energetic (Frederiksen et al., 1992; Freiwald, 2002; Kenyon et al., 2003; Roberts et al., 2009; Masson et al., 2003; Findlay et al., 2014). Finally, modern distributions of CWC seem to be strongly related to the supply of organic matter (Davies et al., 2009) and bottom currents that permit coral larvae dispersal, maintain (food) particles in suspension and prevent corals from being smothered by sediment (Mienis et al., 2007, 2009; Somoza et al., 2014; Sanchez et al., 2014).

Due to their critical role in modern marine ecosystems and the potential to use these archives for paleoenvironmental studies (e.g. Robinson et al., 2014) a number of key papers have attempted to understand and reconstruct the growth history of CWC reefs and mounds. These studies mainly based on U-series dating of fossil coral fragments retrieved from carbonate mounds have permitted to establish the late-Quaternary spatial and temporal distribution of CWC in the North Atlantic (Lutringer, 2003; Dorschel et al., 2005; Frank et al., 2009; 2011; López Correa et al., 2012; Douarin et al., 2013; Victorero et al., 2016; Bonneau et al., 2018). A number of growth models of carbonate mounds and reefs have been proposed (Wilson et al., 1979; Kenyon et al., 2003; De Mol et al.,2005; Dorschel et al., 2005; Roberts et al., 2006; Rüggeberg et al., 2007; De Haas et al., 2009; Bonneau et al., 2018; Pirlet et al., 2011). In more detail, it has been demonstrated that interglacial climates were favourable for CWC growth and carbonate mound development, while until present no CWC from glacial periods have been discovered between 50°N and 70°N in the North Atlantic (Schröder-Ritzau et al., 2005; Van der Land et al., 2014; Frank et al., 2009; 2011; Douarin et al., 2013; Bonneau et al., 2018; Matos et al., 2015) nor at 25°N in the Gulf of Mexico (Matos et al., 2018). On the contrary, at temperate latitudes between 20°N and 50°N in the NE Atlantic, glacial periods are associated with increased framework forming CWC reef growth. *Lophelia pertusa* reef growth is reported during glacial periods and cool events such as the Younger Dryas in the Gulf of Cádiz, Mediterranean Sea and off Mauritania (Wienberg et al., 2009; 2010; McCulloch et al., 2010; Eisele et al., 2011; Frank et al., 2011).

Frank et al. (2011) has proposed that such glacial-interglacial changes in the distribution of CWC reefs in the North Atlantic could be linked to the North-South displacement of cold nutrient-rich intermediate waters and surface productivity driven by changes in the position of the polar front. However, other mechanisms could be involved in the emergence of this pattern, such as changes in the temperature and related pycnocline, which is associated with the development of nepheloid layers (Raddatz et al., 2014; Rüggeberg et al., 2016) or changes in detrital input (e.g. ice-rafted debris) (Pirlet et al., 2011; Thierens et al., 2012; Bonneau et al., 2018). The effect of the carbonate chemistry changes and pH and calcium carbonate saturation conditions of the ocean has been shown to have an effect on CWC growth (Hennige et al., 2015; Raddatz et al., 2016). More recently, a compilation of U-series dating of CWC fragments collected in a restricted area of the SW Rockall Trough margin have shown that CWC growth was influenced by millennial-scale North Atlantic climate variability during the late Holocene with systematic lower CWC occurrence during cold events of the late Holocene (Bonneau et al., 2018). A similar study in Mingulay CWC reef also showed that corals were sensitive to periods of rapid climate change (Douarin et al., 2015; Dubois-Dauphin et al., 2019).

In this paper, we investigate a sedimentary record that provides new evidence for the environmental parameters that control the settlement of CWC reefs on the northern margin of the British continental shelf at the end of the last deglaciation. A vibrocore was collected on the continental margin North of Scotland at 282 m water depth. We obtained numerous U/Th and ^{14}C dates on *Lophelia pertusa* (12 of which are paired), and ^{14}C dates on bivalves (*Venus casima* and other *Venus* sp.) and foraminifera (*Cibicides refulgens*). We also derived a stable isotope profile from planktonic species *Globigerina bulloides*. Clay mineralogical composition and laser grain-size distribution were measured in order to relate changes in sediment sources and dynamic of transport with the appearance of the CWC reef at this location.

2. Material and Methods

2.1 Sediment core location

The British Geological Survey (BGS) vibrocore +59-07/293VE was retrieved from the UK continental shelf, at the junction with the Wyville Thomson Ridge and the West Shetland shelf / Hebridean shelf (59°43.40N; 06°28.90W, 282 m water depth) during a regional mapping survey on board the MV British Enterprise Four (Long et al., 1999; (Figure 1)). Initial observations of CWC presence at the study site were obtained in the 19th century (e.g. Wyville-Thomson, 1874). More recently the area was surveyed and the distribution of CWC mapped (Long et al., 1999). Results from this survey showed the presence of living reefs of *Lophelia pertusa* down to a maximum water depth of 500 m with a maximum presence of living reefs centred between 300-400 m (Roberts et al., 2003; Long et al., 1999), but only dead CWC were observed at the study site. Processes governing sedimentation in this area have been studied and show complex interactions between bathymetry and bottom-water currents (Howe et al., 2002).

The total recovery of vibrocore +59-07/293VE was 495 cm. Prior to sub-sampling, the core was cut frozen with a diamond saw, in order to keep the internal sedimentary structure intact. The top 300 cm of the core presented extremely abundant fragments of *L. pertusa*, up to 9 cm length. A one meter section of the core, between 61.5 to 161 cm, is highly disturbed with only small < 1 cm, highly fragmented and eroded *L. pertusa* samples. The bottom section, from 300-495 cm, presents no coral fragments. The biogenic fraction is composed of diverse bivalves, benthic and planktonic foraminifera and numerous well-rounded glaciomarine rock fragments. The coral-rich section of the core was sampled at 10 cm intervals, documenting the position and state of preservation of each coral fragment. The bottom 195 cm of the core were sampled at 5 cm intervals. Clay mineralogical analyses were performed on clay-sized fraction and laser grain-size analyses were conducted after removal of carbonate and organic matter. Stable isotopes ($\delta^{18}O$) of *Globigerina bulloides* were measured on sieved sediment samples. U/Th and ^{14}C analyses were done on selected fragments of corals sampled at specific depths down core.

2.2. Hydrological setting

The site investigated is located on the path of the North Atlantic Current (NAC) (Figure 1). As the NAC flows northwards it mixes with the European Shelf Edge Current (SEC) (Marsh et al., 2017; Inall et al., 2009; McCartney and Mauritzen, 2001). The SEC forms a northward-flowing boundary current centered at 200 m depth that brings warm and saline upper water with Eastern North Atlantic Central Water (ENACW) characteristics along the European margin to the Faroe-Shetland Channel (Holliday et al., 2000; White and Bowyer, 1997; Hill and Mitchelson-Jacob, 1992; Ellett et al., 1986; Pollard et al., 2004) (Figure 1). In addition, the Scottish Coastal Current (SCC), which flows on the shelf margin, mixes with SEC potentially indirectly affecting flow patterns at our study site (Inall et al., 2009; Ellet et al. 1986, 1979). The Scottish Coastal Current (SCC) brings cooler and fresher waters from the Irish and Clyde Seas (Ellett and Edwards, 1983). In the deeper section of this channel colder waters flow: Arctic Intermediate Waters (AIW) and Norwegian Sea Arctic Intermediate Waters (NSAIW), which appear to control the lowest depth habitat of *L. pertusa* in this area (Roberts et al., 2003).

2.3 Sampling for U/Th and ^{14}C dates

In total, 43 downcore pristine fossils of *L. pertusa* were selected for U/Th dating (Table 1). A 3-4 g piece of each coral fragment was ultrasonically cleaned in MilliQ water 3 times, as done in (Douarin et al., 2013), to avoid contamination from sediment and surface deposit. Inner and outer surfaces of CWC samples were carefully cleaned using a small diamond blade to avoid contamination from iron and manganese oxides/hydroxides and surface sample re-crystallisation of aragonite into calcite. The coral fragments were then sub-sampled for X-ray diffraction (XRD) analysis for mineralogical analysis (aragonite content). The XRD analysis was performed at GEOPS and confirmed that the cleaned corals were made of 100% aragonite. Pristine coral samples were dated by ^{14}C and U-series methods. The amount of material for each coral was larger than required to account for potential duplicates or other analytic work.

2.4. AMS ^{14}C dates

Coral fragments are only present from the core top to 300 cm and thereafter bivalves and foraminifera were used for ^{14}C dates. A total of 26 radiocarbon Accelerator Mass Spectrometry (AMS) ages were obtained on a range of material : 17 CWC, 3 marine bivalve fragments, 6 foraminifera *C. refulgens* samples (Table 1). For each ^{14}C date about 10 mg of $CaCO_3$ is required. When possible we used the subsamples of the same *L. pertusa* coral fragments used for U/Th dates. For the foraminifera, specimens of benthic foraminifera *C. refulgens* were hand-picked from the 250-1000 µm fraction of the sediment. Fragments of marine bivalves (*Venus casima* and other *Venus* sp.) were selected and cleaned. All ^{14}C ages were calibrated with CALIB 7 program using the calibration curve Marine13 and assuming a mean constant surface ocean reservoir age of 400 years (Stuiver et al., 2005; Reimer et al., 2013).

2.5. U/Th dates

The CWC fragments selected were U-series dated at the Laboratoire des Sciences du Climat et de l'Environnement (LSCE, CEA-CNRS-UVSQ, Gif-sur-Yvette). 43

L. pertusa samples were analysed for uranium and thorium isotopes using a Multi-Collector Inductively Coupled Plasma Mass Spectrometer MC-ICP-MS. Prior to analyses, all fragments were examined under a binocular microscope to ensure against the presence of bio-eroded zones and finally crushed into a coarse-grained powder with an agate mortar and pestle. The powders (~60-200 mg) were transferred to acid cleaned Teflon beakers, ultrasonicated in MilliQ water, leached with 0.01 N HCl for around 15 s and finally rinsed twice with MilliQ water. The U and Th separation and purification followed a procedure modified from Pons-Branchu et al. (2005) and Douville et al. (2010). The physically and chemically cleaned samples were dissolved in 3-4 ml dilute HCl (~10%) and mixed with an internal triple spike with known concentrations of ^{229}Th, ^{233}U and ^{236}U, calibrated against a Harwell Uraninite solution (HU-1) assumed to be at secular equilibrium (Frank et al., 2004). After Fe-coprecipitation, the U and Th fractions were separated and purified on 600 l columns packed with U-TEVA and prefilter resins in nitric media. The U and Th isotope ratios were determined using a Thermo ScientificTM MC-ICP-MS fitted with a desolvating introduction system (aridus II) following the procedure described by Pons-Branchu et al. (2014). The 230Th/U ages were calculated from measured atomic ratios through iterative age estimation (Ludwig and Titterington, 1994), using the ^{230}Th, ^{234}U and ^{238}U decay constants of Cheng et al. (2013) and Jaffey et al. (1971).

2.6. Stable isotopes: *G. bulloides* δ^{18}O and δ^{13}C profiles

About 10-20 specimens of *G. bulloides* (250-400 μm) were hand-picked at a 10 cm resolution from 0-300 cm and thereafter a 5 cm resolution. Samples were analysed at LSCE (CEA-CNRS-UVSQ, Gif-sur-Yvette) using an OPTIMA GV mass spectrometer with a common acid bath automatic preparation line. Shell oxygen isotope values are expressed relative to the isotopic ratio of the carbon dioxide gas derived from the Vienna Pee Dee Belemnite (VPDB) standard in conventional delta notation (δ). Ratios are reported in ‰ VPDB defined with respect to the NBS 19 ($\delta^{18}O$ = -2.20‰ VPDB), limestone standard. The mean external reproducibility (1) of carbonate standard is ±0.06% for $\delta^{18}O$ and ±0.04% for $\delta^{13}C$.

2.7. Clay mineralogical analyses

A total of 69 sediment samples collected from the vibrocore +59-07/293VE were used for clay mineralogical analyses. The clay minerals were identified by XRD using a PANalytical diffractometer at the GEOPS laboratory (Université Paris-Saclay, France) on oriented mounts of non-calcareous clay-sized (< 2 μm) particles. Briefly, deflocculation was accomplished by successive washing with distilled water after removing carbonate and organic matter by treating with acetic acid (25%) and hydrogen peroxide (15%), respectively. The particles smaller than

2 m were separated by sedimentation and centrifugation. Three XRD runs were performed, following air-drying, ethylene-glycol solvation for 24 hours, and heating at 490°C for 2 hours. The clay minerals were identified according to the position of the (001) series of basal reflections on the three XRD diagrams. Mixed layers composed mainly of smectite-illite (15-17 √Ö) were included in the "smectite" category. Semi-quantitative estimates of peak areas of the basal reflections for the main clay mineral groups of smectite (15-17 √Ö), illite (10 √Ö), and kaolinite/chlorite (7 √Ö) were performed on the glycolated curve using the MacDiff software. The relative proportions of kaolinite and chlorite were determined based on the ratio from the 3.57/3.54 √Ö peak areas. The replicate analyses of a few selected samples gave a precision of ¬±2% (2). Based on the XRD method, the semi-quantitative evaluation of each clay mineral had an accuracy of ~4%.

2.8. Laser grain-size analyses

Grain-size distribution measurements in the range of 0.02 to 2000 Œºm were carried out on a Malvern Mastersizer 2000 Particle Size Analyzer on the same samples as those analysed by XRD. Prior to the analyses, bulk sediment was pre-treated with acetic acid (25%) and hydrogen peroxide (15%) to remove carbonates and organic matter. The mixture was then rinsed several times with deionized water and gently shaken to achieve disaggregation. The suspension was then poured into the fluid module of the particle size analyser.

The total set of grain-size distributions (n=69) has been summarized by an unmixing algorithm in order to estimate sediment sub-populations representing different sources or dispersal processes. This approach has been significantly improved by the last generation of unsupervised linear unmixing under positivity and sum-to-one constraints (Weltje, 1997). We used the Bayesian Positive Source Separation (BPSS) algorithm that has the main advantage of having robust convergence properties (Moussaoui et al., 2006; Dobigeon et al., 2009; Schmidt et al., 2010). We estimate both the grain-size distributions of each sub-population (end-members) and the proportion of each end-member through time. The number of end-members is estimated by the best trade-off between variance reconstruction and end-member significance.

3. Results

3.1. Chronology and age model

All U/Th and ^{14}C dates are plotted against sediment core depth (Figure 2, (see also Figure 4), Table 1, Table 2). A total of 43 U/Th and 17 ^{14}C dates were obtained on *L. pertusa* samples from this sediment core. Additional ^{14}C dates were obtained from 6 benthic foraminifera samples (*Cibicides refulgens*) and on 3 bivalves. Results show that *L. pertusa* U/Th dates are spread more or less evenly downcore and regularly increase from 2 to 8 ka BP down to 272 cm (Table 2). However, after 272 cm U/Th dates start decreasing again to 5.6 ka at 306 cm (Table 2, Figure 2). Similarly, *L. pertusa* ^{14}C dates regularly increase from the core top to 310 cm ranging from 2.5 to 8.45 cal ka BP. The *C. refulgens* ^{14}C dates also regularly increase from 40 to 306 cm ranging from 5.4 to 10.3 cal ka BP. In the bottom section of the core, from 385-480 cm, ^{14}C dates are much older 23-40.7 cal ka BP (Table 1, Table 2, Figure 2). Finally, three ^{14}C dates were obtained from selected samples of marine bivalves, *Venus casima* and *Venus* sp. The ages also increase with depth from 10.7 at 308 cm to 27.4 at 425 cm. The sample selected at 480 cm has an age older than 50 cal ka BP. We firstly observed an absence of well-preserved coral fragments in the core from 61.5 to 160.5 cm and we were unable to obtained reliable U/Th or ^{14}C dates. Secondly, we observed very significant age offsets between the U/Th and the ^{14}C dates (Figure 2, Table 1, Table 2, Figure 4).

We conducted multiple analyses to test for any geochemical or physical alteration. All the samples presented in this work have passed the standard checks for U/Th and ^{14}C quality. Each sample was analysed for XRD and underwent thorough cleaning and leaching procedures. Replicate analysis were conducted on several samples for U/Th (Table 2), and we analysed twice the same solution (tests for analytical reproducibility) and obtained similar ages. For the replicates at 293 cm and 306 cm (Table 2), the U/Th analyses were done on different pieces of the same coral. A little age difference around 140 years for the sample at 293 cm, or more important around 400 years for sample 306 cm (5.20 ¬± 0.04 and 5.59 ¬± 0.03 ka BP, Table 2) is found for U/Th dating (Table 1). Similarly, the ^{14}C analyses were run in two separate batches (starred and non-starred samples on Table 1). Comparable results are found at similar depth: for example 4.8 cal ka BP at 38.5cm and 4.7 cal ka BP at 39 cm; 8.4 cal ka BP at 268 cm and 8.4 cal ka BP at 272 cm. Similar ages are also obtained for coral, foraminifera and bivalve samples from the same sediment depth (for example *C. refulgens* at 250 cm at 8.2 cal ka BP and *L. pertusa* at 247cm at 8.4 cal ka BP). Based on all available data and results, we conclude that there is no clear evidence for any geochemical or physical alteration which may have explained the observed offset between U/Th ages and ^{14}C ages.

Given that there appears to be an unexplainable significant discrepancy between the U/Th ages and the ^{14}C ages, we decided to use the $\delta^{18}O$ profile as a guide to build an age model. $\delta^{18}O$ values range from 2.5 to 1‰ from the base of the core to the top (see Figure 4). These data are compared to a well-dated sediment core from the North Atlantic (Na87-22, see Figure 5).

3.2. Siliciclastic grain size

Grain size of siliciclastic particles in vibrocore +59-07/293VE ranges from 0.6 to 800 ¬µm and the mean grain size varies from 19 to 100 ¬µm (average ~42 ¬µm) (Figure 3). In general, the mean grain size presents higher values in the core section 300-485 cm (Figure 3). The inversion algorithm for end-member modelling of composition data for core +59-07/293VE displays a three end-member model that explains more than 80% of the variance. The coarse end member EM3 varies within the size range 0.6 to 800 ¬µm (bi-modal grain size of ~5 and 110 ¬µm) (Figure 3). The intermediate end member EM1 varies in the size range 2-141 ¬µm, with a modal grain size of ~20 ¬µm. The fine end-member EM2 varies in the size range 1-141 ¬µm, and its modal grain size is ~6 ¬µm. These last two end-members (EM1 and EM2) present a clearly defined unimodal distribution. Relative contributions of the three end-members are plotted against age in Figure 3. Proportions of the coarser end-member (EM3) display a large range of variation, between 0 and 87%, with an average value of ~31%. Proportions of the intermediate end-member (EM1) vary in a range, from 0 to 65% (average ~27%). The last end-member (EM2), which represents the finer particles, varies between 0 and 80% (average 41%). The intermediate EM1 presents a higher percentage variability with no systematic change downcore.

The mean grain size is strongly influenced by the proportions of the coarse EM3 (Figure 3). The evolution of the proportion of EM1 and EM3 shows a significant shift at around 300 cm. The coarser EM1 presents a higher percentage (from 20 to 87%, with an average value of ~48%) below 300 cm than in the upper part of the core (from 0 to 20%, with an average value of ~9%). In contrast, proportions of EM2 are lower (from 0 to 54%, with an average value of ~29%) below 300 cm than thereafter (from 16 to 79%, with an average value of ~58%).

3.3. Clay mineralogy

In core +59-07/293VE, smectite (15-97%) and illite (1.5-49%) are the dominant clay minerals while chlorite (1.5-26%) and kaolinite (1-19%) are present in lesser quantities (Figure 4). In general, illite, chlorite and kaolinite contents display relatively similar distributions and are inversely correlated to smectite contents. In the bottom section of the core (corresponding to the interval depth from 480 to 300 cm) the clay fraction is characterized by higher proportions of smectite (from 96 to 35%) and lower contents of illite (from 0.5 to 35%), chlorite (from 0.5 to 25%) and kaolinite (from 0.5 to 13%) when compared to the upper 300 cm.

In detail, between 485-410 cm, smectite content displays higher values (from around 92 to 96%), before rapidly decreasing to 54% at 410 cm. This decrease in smectite content is associated with an increase in illite and chlorite content, from 0.5 to 25% and 0.5 to 14%, respectively. In the core section from 390 cm to the core top, the proportions of smectite continue to decrease rapidly from 54% to 35 % followed by a maximum of smectite (57%) around 315 cm. Thereafter the smectite content decreases again around 300 cm, when the CWC appear, and decreases progressively from 35 to 10 % to the core top. This general decrease in smectite content in two steps with sharp transitions centred at 300 and 380 cm is associated with an increase in illite, chlorite and kaolinite contents.

4. Discussion

4.1. Potential diagenesis effect and the U/Th and ^{14}C age offset.

The comparison of U/Th and ^{14}C data sets reveals significant differences in the age depth relationships, particularly between 160-306 cm (Figures 2, 4 and Tables 1, 2) where differences in age of up to 2500-1500 years can be observed. A total of 12 paired U/Th and ^{14}C dates enable to estimate reservoir ages following similar approach as in previous studies (Frank et al., 2004; Douarin et al., 2015). Values range from 530 to >3000 years. Most of these reservoir age estimates are outside the natural range in the modern ocean and unexpected in surface waters so close to the area of formation of deep waters in the North Atlantic. In the section between 0-60 cm, above the interval with highly altered corals, three reservoir age estimates are between 530-1050 years, which is closer to the expected values, yet still significantly higher than recent estimates for the Holocene (Cage et al., 2006). We consider that our results attest of an of a diagenetic process that standard quality tests have failed to highlight. We further hypothesise that there could be a relationship between the diagenesis processes and the reworked section of the core between 60-160cm, there are signs of dissolution and no well-preserved CWC fragments were found in this interval. We observe the largest age offsets between ^{14}C and U/Th ages in the core section 160-306 cm, which is just below the reworked layer (Figure 4).

Diagenetic processes in CWC environments have first been observed by Foubert et al., (2007) who proposed that the rapid accumulation (commonly between 50-100 cm/ka) rates in these environments was associated with an elevated oxidation of organic matter, which led to dissolution of aragonitic corals. Early diagenesis observed in sub-modern samples showed significant offsets between recent and older sections of the same coral fragment. However, these age offsets were of smaller magnitude and there was a coherent offset for ^{14}C ages (Pons-Branchu et al., 2005). More recently, other studies have described similar diagenetic processes (Pirlet et al., 2009, Raddatz et al., 2014). Pirlet et al., (2009) highlights the formation of gypsum associated to the oxidation of sedimentary sulphide minerals such as pyrite and the dissolution of carbonates. These authors explained the oxidation by a phase of increased bottom currents which caused erosion and enhanced inflow of oxidizing fluids into the mound sediments. We did not observe any presence of gypsum in our sediment core but further analyses would be required to exclude this possibility. However, both ^{14}C and U/Th dates were performed on the same sediment core as the one used by Pirlet et al., (2009) and results do not show such large age offsets (Frank et al., 2009). It is thus unclear if the oxidation of organic matter can cause modifications of the U/Th or ^{14}C ages. Such a dissolution event may have occurred and could explain the absence of well-preserved CWC in the interval 60-160 cm (Figure 4). However, there are no signs of dissolution of the planktonic and benthic foraminifera which could indicate that if there was dissolution, this would have affected mainly aragonite and not calcite. This diagenetic imprint appears to have affected sediments up to 150 cm below the altered zone which was previously observed in the Challenger mound (Pirlet et al., 2010). The absence of any alterations of the planktonic and benthic foraminifera seems to indicate that this dissolution event may have affected mainly aragonite and not calcite. Interestingly, several studies have previously shown the presence of meter thick sediment layers with similar characteristics and in similar settings. within sedimentary sequences similar to that observed here between 60-160 cm (Figure 4) One of these sites is located with abundant pyrite and dolomite on the Challenger Mound, a meter thick sedimentary layer was enriched in pyrite and dolomite (Raddatz et al., 2014) . Similarly, in a sediment core collected offshore Norway there was an absence of well-preserved coral in a meter-long section (Raddatz et al., 2016). This later study showed suggested evidence for changes in ocean pH which the authors associated with post-glacial meltwater inputs. However, the timing of the observed shift in ocean pH around is older, 5-6 ka BP (determined by U/Th dates) when compared to results from our study site. Further analyses will be required to fully explain the U/Th - ^{14}C offsets presented in this study and any links with sedimentary processes we are observing.

4.2. Chronology of sedimentary deposits on the Wyville Thomson Ridge.

Our strategy has thus been to use the *G. bulloides* $\delta^{18}O$ profiles to build an independent age model for this site based on the principles of isotope stratigraphy. The stable isotope profile of vibrocore +59-07/293VE is compared to the *G. bulloides* $\delta^{18}O$ profile of sediment core Na87-22 (Figure 5), which is a well-dated sediment core located on the Rockall Plateau (Figure 1) (Waelbroeck et al., 2001). The comparison of the two *G. bulloides* $\delta^{18}O$ profiles enabled to build an independent age model based on matching of the isotope profiles (Figure 5). The age depth relationship of this stratigraphic age model can be compared with the U/Th and ^{14}C dates (Figure 5D). On Figure 5D, we consider the 60-160 cm zone to be either a reworked altered mixed sedimentary layer. This first order stratigraphic age model, built by matching *G. bulloides* $\delta^{18}O$ profiles, is based on 5 tie-points. T between the age core top 0 cm in modern or close to modern with and is estimated age around 1.5 cal ka BP . This was the 'best fit' through both the U/Th and ^{14}C dates. At 400 cm we estimated the age at around 13 cal ka BP based on the match between the *G. bulloides* $\delta^{18}O$ profiles (Figure 5). The Finally, the base of the sediment core is considered of glacial age (Figure 5). The accuracy of the age model is variable downcore. The $\delta^{18}O$ transition observed between 300-400 cm enables a more robust age estimate compared to the core top 0-300 cm where a $\delta^{18}O$ plateau is observed. As a result we do not attempt to interpret millennial-scale trends in our data at millennial-scale level, as done in previous studies (e.g. Bonneau et al., 2018 , Colin et al., 2019).

Using this stratigraphic age model, the results of mineralogy and grain-size data highlight three phases in sediment deposition, associated with significant shifts in sedimentation rate. Firstly, glacial age sediment deposits between 400-495 cm (Figure 5), with ages > 50-13 cal ka BP. Secondly, the deglacial sediments accumulate between 306-400 cm (Figure 5), with ages between 13-9 cal ka BP. Thirdly, Holocene sediments are deposited (the past 9 cal ka BP), corresponding to the period of settlement of CWC, between 0-306 cm (Figure 5).

4.2.1. Glacial age sediments (40-13 cal ka BP)

The age of the base of the core, from 495-400 cm (Figure 5), is constrained by four ^{14}C ages derived from marine bivalve fragments and foraminifera (from 22.91 to 40.66 cal ka BP and one age >50 cal ka BP). It dates back to the glacial period. Sedimentation rates are low around 2-3 cm/ka with potential periods of non-deposition or even erosion (Figure 5). During this period, the British ice sheet extended northwards and covered large areas of the continental shelf (Clark et al., 2010). The core site would have been shallower and closer to the shoreline and potentially ice covered. The nearby continental ice sheets covered Scotland (Clark et al., 2010) and the Faroe Islands to the North (Figure 1). Episodes of ice-rafted debris deposits are possible during this period which would explain the presence of well-rounded large rock fragments and low content of biogenic fraction.

4.2.2. Deglacial sediments (13-9 cal ka BP)

The section between 400-306 cm corresponds to the end of the deglaciation/early Holocene and range approximately from 13 to 9 cal ka BP (Figure 5). Mean sedimentation rates increase to around 24 cm/ka. There are no *L. pertusa* fragments indicating that conditions were not yet suitable for CWC reef settlement during this interval. The age of this section of the core is mainly based on correlation of the *G. bulloides* $\delta^{18}O$ profile with core Na-87-22. Several ^{14}C dates are, however, coherent with this stratigraphic age model: a sample of a fossil bivalve at 308 cm (10.65 cal ka BP) and a *C. refulgens* ^{14}C sample at 300 cm (10.27 cal ka BP). However, one ^{14}C sample at 385 cm around 22 cal ka BP is too old and not coherent with the proposed age model. We suggest that this could be due to mixing or bioturbation of older sediments. This period correspond to the end of the Younger Dryas event and the following warm event at the end of this rapid climate cooling.

4.2.3. Settlement of CWC during the Holocene around 9 ka BP

The first well-preserved fossil fragments of *L. pertusa* appear at 306 cm with a clear increase observed after 300 cm (Figure 4). Using the stratigraphic age model the age of this transition is around 9 cal ka BP (Figure 5). The ages obtained from U/Th and ^{14}C on fossil coral samples during this interval differ by several thousand years (Figure 4 and 5). The ages derived from the first dated samples at 306 cm are much younger, at around 5.2-5.6 cal ka BP for U/Th dates, whereas the *L. pertusa* ^{14}C dates are within error of this age estimate around 8.3 cal ka BP. As a result estimated mean sedimentation rates are variable (70-34 cm/ka) and depend on which age model or which data set is used, particularly during the 9-4 cal ka BP interval (Figure 2). In the top 60 cm, both U/Th and ^{14}C show a drop in sedimentation rate after 4-5 cal ka BP to around 7 cm/ka (Figure 5).

The important difference between the ^{14}C and U/Th ages raises some uncertainty on the ages obtained in this section of the core. The chronology proposed based on stable isotope stratigraphy provides an age around 9 cal ka BP for the settlement of the CWC reef. This age is, however, supported by ^{14}C dates 1- *L. pertusa* ^{14}C date at 306 cm of 8.4 cal ka BP, 2- the *C. refulgens* ^{14}C date at 300 cm around 10.3 cal ka BP and 3- the *Venus casima* ^{14}C date at 308 cm is around 10.6 cal ka BP (Table 1). Furthermore, in a nearby site, but in a deeper setting at around 900 m water depth, a slightly older age has been found for the first occurrence of *L. pertusa* at around 10.3 cal ka BP (Victoreo et al., 2016). We consider that these ^{14}C ages are consistent and support the stratigraphic age model proposed here.

4.3. Transition from glacial to deglaciation on the Wyville Thomson Ridge

The glacial age sediment deposits are characterised by high values of mean grain size (Figure 5). Grain-size distributions of the siliciclastic fraction can be used to infer the hydrographic conditions at the time of deposition (e.g. Ballini et al., 2006; Prins et al., 2002) and have already been used to establish past current intensity and the presence of IRD deposits in CWC mound records (e.g. Pirlet et al., 2011; Thierens et al., 2012). The grain-size distribution indicates strong variations in agreement with lithological description and glacial and interglacial changes. Glacial age sediments show a poorly-sorted bimodal grain-size distribution associated with sediments enriched in coarse (>150 m) lithic particles which points towards ice-rafting as a likely transport and sedimentation mechanism (Figure 3). The presence of dropstones (rock fragments up to several centimeters) below 400 cm, confirm that these sediments are of glaciomarine origin.

The grain-size distribution of EM3 characterizes poorly sorted sediments, enriched in the coarser size fractions of up to 800 m, which can be attributed to sediments transported by icebergs (e.g. Prins et al., 2002; Pirlet et al., 2011; Thierens et al., 2012) (Figure 3). EM3 dominates the glacial period indicating a predominance of coarse sediments transported by icebergs most probably from the BIS in agreement with the maximum extent of the continental ice sheets during this period (Figure 1) (Golledge et al., 2008; Clark et al., 2010). In addition, such poorly sorted grain-size distribution during glacial times suggests that the coastal current was sluggish in the studied area and was unable to sort coarse glaciomarine deposits as it was also observed for glacial sediments of CWC mounds of the Porcupine Seabight (Pirlet et al., 2011).

These coarse glacial sediments are associated with high content of smectite that reach up to 96%. Clay mineral assemblages of the high latitude of the North Atlantic can reveal information on the palaeo-environmental conditions that governed continental weathering processes on adjacent landmasses and/or sedimentary sources (e.g. Chamley, 1989; Fagel et al., 1996; Bout-Roumazeilles et al., 1997; Ballini et al., 2006; Pirlet et al., 2011). Sediment distributions and sources in the NE Atlantic have been established in several previous studies (Biscaye, 1965; Latouche, 1975; Windom, 1976; Grousset et al., 1982; Grousset and Para, 1982; Latouche and Para, 1976; Pirlet et al., 2011; Thierens et al., 2012). Clay mineralogical composition of surface sediments of the NE Atlantic (between the Faroe and Shetland Islands and the northern margin of North Scotland) is mainly controlled by the petrology of the eroded source area. The clay fraction of sediments north of the Wyville Thomson Ridge and south of Iceland is characterized by abundant smectites (50-100%) compared to illite (0-30%) deriving from the weathering of basaltic rocks from the Iceland and the Faroe-

Shetland ridge area (e.g. Latouche, 1975; Grousset et al., 1982). The weathering of these volcanic rocks provides large quantities of smectite transported southward by oceanic currents and smectite composes up to 90% of the clay fraction in the sediments surrounding the Iceland and Faroe Islands (Grousset et al., 1982) and on the pathway of deep-current circulating along this volcanic province (e.g. Iceland Scotland Overflow Water; Fagel et al., 1996 ; Ballini et al., 2006 ; Fagel et al., 2006). On the contrary, the clay fraction in sediments from the Scottish and Irish continental shelves has high content in illite (> 50% illite) (Latouche, 1975; Windom et al., 1976) and low smectite concentrations (<20 %) sourced from physical erosion of soils of northern Europe, which developed on crustal rock formations under cold and intermediate climates.

Consequently, the smectite/illite (Sm/I) ratio reported in Figure 5 can be used here to track clay minerals deriving from the weathering of the northern Iceland-Scotland Ridge basalts (smectite) and the more local sources of clay derived from soils developed on crustal rock formations from North Scotland which are transported via river flow and then coastal currents. Similar studies have used this proxy to separate the Icelandic source of the clay fraction from sediments in the North Atlantic at different times scales (e.g. Fagel et al., 1996; Bout-Roumazeilles et al., 1997; Ballini et al., 2006 ; Fagel et al., 2006). In core +59-07/293VE, this mineralogical ratio ranges from 0.2 to 33, with last deglacial sediment values being higher than those for the late Holocene (Figure 5), and is characterized by two abrupt decrease around 13 and 9 ka BP.

The high concentration of smectite in the glacial deposits at the study site implies that clay minerals are mainly sourced from a northern volcanic source such as the Iceland-Scotland Ridge basalts (Ziska and Varming et al 2008). This contrasts significantly with the grain-size data which imply a local source of ice-rafted material most probably from the BIS. A possible explanation is that the ice-rafted material transported small quantities of the illite and chlorite and mainly coarser material as shown by the high values of EM3. This can be explained by a lack of soil produced over the ice covered Scottish continent during glacial periods. The fine sized clay material would be primarily produced during warm interglacial periods and would be rapidly exported during the initial glacial phase in agreement with results obtained by Pirlet et al. (2011) and Thierens et al. (2012) in the Porcupine Seabight. The high values of smectite also imply significant modifications of ocean circulation with possible southward flow of surface waters during glacial periods. This is in agreement with a map of reconstructed surface currents for this area obtained by Sarnthein et al. (1995) indicating that surface currents were flowing southward during the glacial and northward flowing during the Holocene.

At around 13 cal ka BP, there is a sharp transition marked by a reduction of smectite whereas the mean grain size does not change significantly until around 9 cal ka BP (Figure 5). The proportion of EM3 remains high and sediments are still poorly sorted, which means that currents in the study area remained sluggish during this period. The opposing signals observed in the clay mineralogy and grain-size data imply sources and transports of different sedimentary size fractions as described during the glacial periods. During the interval 9-13 cal ka BP, towards the end of the deglaciation, smectite concentrations remain high around 30-40% corresponding to a mixed volcanic northern source and sedimentary material from a southern source. This period 13-9 cal ka BP thus marks a shift in oceanic currents occurs which is at the study site at the end of the deglaciation, and associated with the initiation of shelf currents (SCC and SEC), which flow northwards along the west coast of Scotland and transport the sedimentary material to the study area via (Simson and Hill 1986). In addition, at 9-9 13 cal ka BP, the northern regions of the Scottish mainland were became progressively ice free (Golledge et al., 2008). The soils that developed during the warmer climatic conditions of the early Holocene Such a configuration would have permitted the production and transport by river runoff of a larger quantities of illite and chlorite from soils that developed during the warmer climatic conditions of the early Holocene.

4.4. Cold water reef settlement and sedimentary environment during the early Holocene

The final transition in sediment properties occurs during the early Holocene around 9 cal ka BP when a second significant change in clay mineralogy is associated with a change in mean grain size and a significant increase in sedimentation rates (Figure 5). This transition is coeval with the CWC reef settlement at the study site. There is a strong reduction of the smectite (around 35%, decreasing thereafter to 15%), and a significant increase of both illite (35%, increasing thereafter to 50%) and chlorite (25%) (Figure 5) . These observations attest of a reduction of the northern-sourced smectite and an increase of Scottish-sourced illite and chlorite. The grain-size data shows a sharp reduction of EM3 and an increase of EM2 which implies more energetic bottom-water flow able to sort sediment and the source of the clay sized fraction. We interpret this data as evidence for a sudden change in energy and possibly direction of bottom-water currents around 9 cal ka BP, which we interpret as reflecting an increase in southern sourced oceanic currents (mainly the SEC and the SCC) that bring clay minerals from the coastal areas and the continental shelves surrounding the Scottish mainland. At 9 cal ka BP, the northern regions of the Scottish mainland are ice free (Golledge et al., 2008). Such a configuration would have permitted the production and transport by river runoff of a larger quantity of illite and chlorite from soils .

The meltwater produced by the final decay of the large continental ice sheets has been shown to affect ocean circulation patterns in the North Atlantic, reducing the salinity and the vigour of the North Atlantic Current (and AMOC) until around 8 cal ka BP (Thornalley et al., 2013; Mjell et al., 2013; Hoogakker et al., 2011; Gherardi et al., 2009; Kissel et al., 2013). These changes in salinity are known to have affected the strength of the NAC, which could also have affected the flow regimes of the SCC and SEC in this area. Consequently, the settlement of CWC at 9 cal ka BP seems related to a major shift in North Atlantic circulation patterns. Sortable silt records form sediment cores located south of Iceland show a gradual increase in deep-water circulation observed around 8-6 cal ka BP on the Scotland Iceland overflow water (Mjell et al., 2013; Hoogakker et al., 2011; Thornalley et al., 2013) associated to an intensification and eastward extension of the sub-polar gyre (e.g. Thornalley et al., et al., 2009; Colin et al., in press2019). This transition centred around 8 cal ka BP has been associated with the final decay of the northern hemisphere ice sheets.

5. Conclusions

Results from a vibrocore located on the Wyville Thomson Ridge North of the Scottish continental shelf at 300 m water depth enables to estimate the age of the onset of cold water coral reef growth in this area. Multiple U/Th and ^{14}C dates were derived from fossil *Lophelia pertusa*, marine bivalves and foraminifera. The oldest cold water coral, L. pertusa, fragments dated by ^{14}C and U/Th dates are 8.4 and 7.9 cal ka BP, respectively. However, we observe significant and unexplained differences between paired samples of ^{14}C and U/Th dates, which appear to be affected by a diagenetic effect which we do not yet fully explain. We thus derived an independent age model based on isotope stratigraphy using profiles of $\delta^{18}O$ derived from planktonic species *G. bulloides*. The reconstructed age model enables to provide an independent estimate of the date the onset of reef growth to around 9 cal ka BP, which is coherent with the ^{14}C dates of the oldest CWC sample.

Grain size and clay mineralogy provide information about the evolution of the flow patterns and direction of water currents in this area. These records show 2 marked transitions at around 13 and 9 cal ka BP. We thus identify 3 periods characterised by different clay mineralogy and grain size: a glacial period (prior de 13ka BP), an end of deglaciation (13-9 cal ka BP) and a Holocene section (9 to modern cal ka BP).

The first transition at 13 cal ka BP, is characterized by a shift of smectite-rich, poorly sorted sediments to a mixed clay mineralogy of smectites and illites. This transition marks the end of the glacial period, when clay mineralogy was dominated by smectite (75 to 96%) to the deglaciation when the % smectite reduces to 50%. Such mineralogical changes that can be observed between 13 and 9 cal ka BP indicate large variations of sediment sources from the volcanic province of the Iceland-Faroe Ridge (smectite) to a crustal province of the north of Scotland (illite and chlorite). This period is also associated with a strong decrease of the siliciclastic grain size. Sediments become better sorted which reflects an increase of bottom-current velocity. There is a decrease of IRD deposits linked to the retreat of the northern glacial ice sheet and.

The second transition is clearly associated with the appearance of CWC, *Lophelia pertusa*, at this site. At around 9 cal ka BP, illite and chlorite increase to 49% and 25%, respectively, and the mean grain size reduces and the sediments become well sorted. Our results show that the onset of CWC growth on the Wyville Thomson Ridge occurred around 9 cal ka BP and was associated with changes in ocean circulation patterns in this area. This age corresponds to the final phases of the post glacial sea level rise and final melting of continental ice sheets. The clay mineralogy enables to identify a sudden changes in the flow patterns of bottom-water currents that induces favourable sedimentological and hydrological conditions for coral growth.

Acknowledgements

We would like thank the British Geological Survey for granting access to sediment core material. The research leading to this study has received funding from the French National Research Agency "Investissement d'Avenir" (n¬∞ANR-10-LABX-0018), the HAMOC project ANR-13-BS06-0003, and the Region Pays de Loire (New Research Group initiative). We thank the Andres Rüggeberg and one anonymous reviewer for their constructive comments which helped improve the quality of the paper. We also thank Marc de Batist for his editorial handling of the manuscript.

References:

Ballini, M., Kissel, C., Colin, C., Richter, T., Dokken T. (2006) Deep-water mass source and dynamic associated to rapid climatic variations during the last glacial stage in North Atlantic: a multi-proxy investigation of the detrital fraction of deep-sea sediments, Geochemistry, Geophysics and Geosystems, 7, Q02N01, doi:10.1029/2005GC001070.

Baltzer A., Bates R., Mokeddem Z., Clet-Pellerin M., Walter-Simonnet A-V, Bonnot-Courtois C. & Austin W.N. (2010) Using seismic facies and pollen analyses to evaluate climatically driven change in a Scottish sea loch (fjord) over the last 20 ka. in Howe, J. A., Austin, W. E. N., Forwick, M. & Paetzel, M. (eds) Fjord Systems and Archives. Geological Society, London, Special Publications, 344, 357-371

Biscaye, P.E. (1965) Mineralogy and sedimentation of the Recent Deep-Sea Clay in the Atlantic Ocean and Adjacent Seas and Oceans, Geol. Soc. Am. Bull. 76.

Bonneau L., Colin C., Pons-Branchu E., Mienis F., Tisnerat-Laborde N., Blamart D., Elliot M., Collart T., Frank N., Foliot L., Douville E. (2018) Imprint of Holocene climate variability on cold-water coral reef growth at the SW Rockall Trough margin, NE Atlantic. Geochemistry, Geophysics, Geosystems.

Bout-Roumazeilles, V. et al. (1997): Latitudinal control of astronomical forcing parameters on the high-resolution clay mineral distribution in the 45¬∞-60¬∞ N range in the North Atlantic Ocean during the past 300,000 years. Paleoceanography, 12(5), 671-686

Chamley, H. (1989) Clay Sedimentology, Springer-Verlag, New-York. 623 pp.

Cheng, H., Lawrence Edwards, R., Shen, C.-C., Polyak, V. J., Asmerom, Y., Woodhead, J. D., Hellstrom, J., Wang, Y., Kong, X., Spötl, C., Wang, X., & Calvin Alexander, E. (2013), Improvements in 230Th dating, 230Th and 234U half-life values, and U-Th isotopic measurements by multi-collector inductively coupled plasma mass spectrometry, Earth Planet. Sci. Lett., 371-372, 82-91

Clark C. D., Hughes A.L.C., Greenwood S.L., Jordan C., Sejrup H.P., (2012) Pattern and timing of retreat of the last British-Irish Ice Sheet, Quaternary Science Reviews, 44, 112-146.

Christophe Colin, Nadine Tisnérat-Laborde, Furu Mienis, Tim Collart, Edwige Pons-Branchu, Quentin Dubois-Dauphin, Norbert Frank, Arnaud Dapoigny, Mohamed Ayache, Didier Swingedouw, Jean-Claude Dutay, Frédérique Eynaud, Maxime Debret, Dominique Blamart, Eric Douville (2019). Millennial-scale variations of the Holocene North Atlantic mid-depth gyre inferred from radiocarbon and neodymium isotopes in cold water corals, Quaternary Science Reviews, 211, 93-106,

Davies, A.J., Wisshak, M., Orr, J.C., & Roberts, J.M. (2008), Predicting suitable habitat for the cold-water coral *Lophelia pertusa* (Scleractinia). Deep Sea Res., Part I, 55, 1048-1062.

Quentin Dubois-Dauphin, Christophe Colin, Mary Elliot, Arnaud Dapoigny, Eric Douville, (2019) Holocene shifts in sub-surface water circulation of the North-East Atlantic inferred from Nd isotopic composition in cold-water corals, Marine Geology, 410, 135-145.

De Haas, H., Mienis, F., Frank, N., Richter, T.O., Steinacher, R., de Stigter, H., van der Land, C., & van Weering, T.C.E. (2009), Morphology and sedimentology of (clustered) cold-water coral mounds at the south Rockall Trough margins, NE Atlantic Ocean. Facies, 55, 1-26.

De Mol, L., Van Rooij, D., Pirlet, H., Greinert, J., Frank, N., Quemmerais, F., Henriet, J.P., (2011). Cold-water coral habitats in the Penmarc'h and Guilvinec Canyons (Bay of Biscay): Deep-water versus shallow-water settings. Marine Geology, 282(1-2), 40-52.

Dobigeon, N., Moussaoui, S., Tourneret, J.-Y., Carteret, C., (2009). Bayesian separation of spectral sources under non-negativity and full additivity constraints, Signal Processing, 89, 2657-2669.

Dorschel, B., Hebbeln, D., Rüggeberg, A., Dullo, C., & Freiwald, A. (2005), Growth and erosion of a cold-water coral covered carbonate mound in the Northeast Atlantic during the Late Pleistocene and Holocene. Earth and Planetary Science Letters, 233, 33-44.

Douarin, M., Elliot, M., Noble, S.R., Sinclair, D., Henry, L.-A., Long, D., Moreton, S.G., & Roberts J.M. (2013), Growth of north-east Atlantic cold water coral reefs and mounds during the Holocene: A high resolution U-series and ^{14}C chronology, Earth Planet. Sci. Lett., 375, 176-187.

Douarin, M., M. Elliot, D. Sinclair, S.G. Moreton, S.R. Noble, D. Long, and J.M. Roberts (2015) "North Atlantic Ecosystem Sensitivity to Shifts in Meridional Overturning Circulation" Geophys. Res. Lett., 42, doi:10.1002/2015GL065999, 2015.

Douville, E., Sall√©, E., Frank, N., Eisele, M., Pons-Branchu, E., & Ayrault, S. (2010), Rapid and precise 230Th/U dating of ancient carbonates using Inductively Coupled Plasma - Quadrupole Mass Spectrometry. Chem. Geol., 272, 1-11.

Dons C (1944) Norges korallrev. K Nor Videns Selsk Forh 16: 37-82

Dullo, C., Fl√∂gel, S., & Rüggeberg, A. (2008), Cold-water coral growth in relation to the hydrography of the Celtic and Nordic European continental margin. Marine Ecology Progress Series, 371, 165-176.

Eisele, Marku.s, & Frank, Norbert F., & Wienberg, Claudia C.,& Hebbeln, Dierk D., & L√≥pez Correa, Matthias M., & Douville, Eric E. and& Freiwald, Andre. (2011). Productivity controlled cold-water coral growth periods during the last glacial off Mauritania. Marine Geology. 280. 143-149. 10.1016/j.margeo.2010.12.007.

Ellett, D.J., (1979). Some oceanographic features of Hebridean waters. Proceedings of the Royal Society of Edinburgh, vol. 77B, pp. 61-74.

Ellett, D.J., & Edwards, A. (1983). Oceanography and inshore hydrography of the Inner Hebrides. Proceedings of the Royal Society of Edinburgh. Section B. Biological Sciences. 83. 10.1017/S0269727000013385.

Ellett, D.J., Edwards, A., & Bowers, R. (1986), The hydrography of the Rockall Channel - An overview. Proc. R. Soc. Edinburgh, Sect. B, Biol. Sci., 88, 61-81.

Fagel, N., Robert, C., and Hillaire-Marcel, C. (1996), Clay mineral signature of the NW Atlantic Boundary Undercurrent, Marine Geology, 130, 19-28.

Findlay, H.S., Hennige, S.J., Wicks, L.C., Navas, J.M., Woodward, E.M.S., and& Roberts, J.M. (2014), Fine-scale nutrient and carbonate system dynamics around cold-water coral reefs in the northeast Atlantic. Scientific Reports, 4, DOI: 10.1038/srep03671.

Foubert, A., Van Rooij, D., Blamart, D. and Henriet, J.-P. (2007) X-ray imagery and physical core logging as a proxy of the content sediment cores in cold-water coral mound provinces: a case study from Porcupine Seabight, SW of Ireland. Int. J. Earth Sci. (Geol. Rundsch.), 96, 141-158.

Frank, N., Paterne, M., Ayliffe, L., van Weering, T., Henriet, J.-P., and Blamart, D., (2004). Eastern North Atlantic deep-sea corals: tracing upper intermediate water ^{14}C during the Holocene. Earth Planet. Sci. Lett. 219, 297-309.

Frank, N., Ricard, E., Paquet, A., van der Land, C., Colin, C., Blamart, D., Foubert, A., Van Rooij, D., Henriet, J.-P., de Haas, H., and& van Weering, T. (2009), The Holocene occurrence of cold water corals in the NE Atlantic: implications for coral carbonate mound evolution. Marine Geology, 266, 129-142.

Frank, N., Freiwald A., Matthias López Correa M., Wienberg C., Eisele M., Hebbeln D., Van Rooij D., Henriet J.-P. Colin C., van Weering T., de Haas H., Buhl-Mortensen P., Murray Roberts J., De Mol B., Douville E., Blamart D., and& Hatt√© C. (2011), Northeastern Atlantic cold-water coral reefs and climate. Geology, 39, 743-746.

Frederiksen, R., A. Jensen, and H. Westerberg. (1992). The distribution of the scleractinian coral *Lophelia pertusa* around the Faeroe islands and the relation to internal tidal mixing. Sarsia 77:157-171.

Freiwald, A. (2002), Reef-forming cold-water corals, in Ocean Margin Systems, edited by G. Wefer et al., pp. 365-385 , Springer, Berlin.

Freiwald, A., Fosså, J.H., Grehan, A., Koslow, T., and Roberts, J.M. (2004), Cold-water coral reefs: out of sight - no longer out of mind. Biodiversity Series 22. Cambridge (UK): UNEP World Conservation Monitoring Centre. 86 pp.

Freiwald, A., Rogers, A., Hall-Spencer, J., Guinotte, J.M., Davies, A.J., Yesson, C., Martin, C.S., and Weatherdon, L.V. (2017), Global distribution of cold-water corals (version 3.0). Second update to the dataset in Freiwald et al. (2004) by

UNEP-WCMC, in collaboration with Andre Freiwald and John Guinotte. Cambridge (UK): UNEP World Conservation Monitoring Centre.

Gherardi, J.M., Labeyrie, L., Nave, S., Francois, R., McManus, J.F. and, Cortijo, E., (2009). Glacial-interglacial circulation changes inferred from Pa-231/Th-230 sedimentary record in the North Atlantic region. Paleoceanography 24.

Grousset, F., Latouche, C., and Parra, M. (1982). Late Quaternary sedimentation between the Gibbs fracture and the Greenland basin : mineralogical and geochemical data. Mar. Geo., 47, 303-330.

Grousset, F., Parra, M. (1982) Contribution of mineralogical and geochemical data to the study of northeast Atlantic deep quaternary sediments : trace-elements as bottom current indicators, Sedim. Geol. 31, 49-61

Golledge N.R. et al. (2008) High-resolution numerical simulation of Younger Dryas glaciation in Scotland. Quaternary Science Reviews 27 (2008) 888-904

Hennige S.J., Wicks L.C., Kamenos N.A., Perna G., Findlay H.S., Roberts J.M. (2015) Hidden impacts of ocean acidificationto live and dead coral framework. Proc. R. Soc. B 282

Henriet J.P., De Mol B., Pillen S., Vanneste M. and others (1998) Gas hydrate crystals may help build reefs. Nature 391: 648-649

Henry, L.-A., Frank, N., Hebbeln, D., Wienberg, C., Robinson, L., de Flierdt, T. Van, Dahl, M., Douarin, M., Morrison, C.L., Correa, M.L., Rogers, A.D., Ruckelshausen, M., Roberts, J.M., (2014). Global ocean conveyor lowers extinction risk in the deep sea. Deep-Sea Res. I Oceanogr. Res. Pap. 88, 8-16.

Hill A.E. and Mitchelson-Jacob E.G. (1993) Observations of a poleward-flowing saline core on the continental slope west of Scotland. Deep Sea Research42 (7), 1521-1527.

Holliday, N.P., Pollard, R.T., Read, J.F., and Leach, H. (2000), Water mass properties and fluxes in the Rockall Trough, 1975 to 1998. Deep-Sea Research, 47, 1303-1332.

Hoogakker, B.A.A., Chapman, M.R., McCave, I.N., Hillaire-Marcel, C., Ellison, C.R.W., Hall, I.R. and Telford, R.J., 2011. Dynamics of North Atlantic Deep Water masses during the Holocene. Paleoceanography, 26, 1-10.

Howe, J.A., Dove, D., Bradwell, T. and Gafeira, J., (2012). Submarine geomorphology and glacial history of the Sea of the Hebrides, UK. Mar. Geol. 315-318, 64-76.

Inall M., Gillibrand P., Griffiths, C., MacDougal, N., Blackwell, K. (2009) On the oceanographic variability of the North-West European Shelf to the West of Scotland. Journal of Marine Systems 77 (2009) 210-226.

Jaffey, A.H., Flynn, K.F., Glendenin, L.E., Bentley, W.C., & Essling, A.M. (1971), Precision measurements of half-lives and specific activities of 235U and 238U. Phys. Rev. C, 4(5), 1889-1906.

Kenyon, N.H., Akhmetzhanov, A.M., Wheeler, A.J., Van Weering, T.C.E., De Haas, H., & Ivanov, K. (2003), Giant carbonate mud mounds in the southern Rockall Trough. Marine Geology, 195, 5-30.

Kissel, C. et al. (2013) Variations in the strength of the North Atlantic bottom water during Holocene Earth and Planetary Science Letters 369-370, 248-259

Lambeck, K.; Rouby, H.; Purcell, A.; Sun, Y.; Sambridge, M. Sea level and ice volume since the glacial maximum Proceedings of the National Academy of Sciences Oct 2014, 111 (43) 15296-15303;

Latouche, C. (1975) Les min√©raux argileux des sediments actuels de l'Atlantique Nord Oriental et du Sud de la mer de Norv√©ge. Proceeding of the Interntional Clay Conference.

Latouche, C., Parra, M. (1976) Mineralogie et geochimie des sediments quaternaires de l'Ocean Atlantique nord-oriental (Mer de Norv√®ge - golfe de Gascogne) - essais d'interpr√©tations sedimentologiques, Mar. Geol. 22, 33-69.

Le Danois E. (1948) La profondeur de la mer. Payot, Paris

Long, D., Roberts, J.M., Gillespie, E.J., (1999). Occurrences of *Lophelia pertusa* on the Atlantic margin. British Geological Survey Report WB/99/24, Edinburgh, 23pp and appendices.

Lopez-Correa, M., Montagna, P., Joseph, N., Ruggeberg, A., Fietzke, J., Flogel, S., Dorschel, B., Goldstein, S. L., Wheeler, A., & Freiwald, A. (2012), Preboreal onset of cold-water coral growth beyond the Arctic Circle revealed by coupled radiocarbon and U-series dating and neodymium isotopes. Quaternary Science Reviews, 34, 24-43.

Ludwig, K.R., & Titterington, D.M. (1994), Calculation of 230Th/U isochrons, ages, and errors, Geochim. Cosmochim. Acta, 58(22), 5031-5042.

Lutringer, A. (2003), Reconstitution de la variabilité des eaux intermédiaires par l'étude de la géochimie des coraux profonds. PhD Thesis, University of Paris XI, 234p.

Marsh R. et al.: Large-scale forcing of the European Slope Current and associated inflows to the North Sea Ocean Sci., 13, 315-335, 2017

Matos et al. (2017) Coral mound development at the Campeche cold-water coral province, southern Gulf of Mexico: Implications of Antarctic Intermediate Water increased influence during interglacials Cape Lookout Cape Lookout

Matos, L., Mienis, F., Wienberg, C., Frank, N., Kwiatkowski, C., Groeneveld, J., Thil, F., Abrantes, F., Cunha, M.R., Hebbeln, D., (2015). Interglacial occurrence of cold-water corals off Cape Lookout (NW Atlantic): first evidence of the Gulf Stream influence. Deep-Sea Res. I Oceanogr. Res. Pap. 105, 158-170.

McCartney M.S., Mauritzen, C. (2001) On the origin of the warm inflow to the Nordic Seas Progress in Oceanography 51, 125-214

McCulloch M., Taviani M., Montagna P., Lopez-Correa M., Remia A., Mortimer, G. (2010). Proliferation and demise of deep-sea corals in the Mediterranean during the Younger Dryas. Earth and Planetary Science Letters. 298. 143-152. 10.1016/j.epsl.2010.07.036.

Mjell T., Ninnemann U., Eldevik T., Kleiven H (2015). Holocene multidecadal- to millennial-scale variations in Iceland-Scotland overflow and their relationship to climate. Paleoceanography. 30. n/a-n/a. 10.1002/2014PA002737.

Mokeddem Z., Baltzer A., Goubert E & Clet-Pellerin M. (2010) A multiproxy palaeoenvironmental reconstruction of Loch Sunart (NW Scotland) since the Last Glacial Maximum in Howe, J. A., Austin, W. E. N., Forwick, M. & Paetzel, M. (eds) Fjord Systems and Archives. Geological Society, London, Special Publications, 344, 343-355.

Masson, D.G., Bett, B.J., Billett, D.S.M., Jacobs, C.L., Wheeler, A.J., & Wynn R.B. (2003), The origin of deep-water, coral-topped mounds in the northern Rockall Trough, Northeast Atlantic. Marine Geology, 194, 159-180.

Mienis, F., De Stigter, H.C., White, M., Duineveld, G., De Haas, H., & Van Weering, T.C.E. (2007), Hydrodynamic controls on cold-water coral growth and carbonate-mound development at the SW and SE Rockall Trough Margin, NE Atlantic Ocean. Deep-Sea Res. I, 54, 1655-1674.

Mienis, F., van der Land, C., de Stigter, H.C., van de Vorstenbosch, M., de Haas, H., Richter, T., & van Weering T.C.E. (2009), Sediment accumulation on a cold-water carbonate mound at the Southwest Rockall Trough margin. Marine Geology, 265, 40-50.

Moussaoui, S., Brie, D., Mohammad-Djafari, A., Carteret, C., 2006. Separation of Non-Negative Mixture of Non-Negative Sources Using a Bayesian Approach and MCMC Sampling, IEEE Transactions on Signal Processing, 54, 4133-4145.

Pirlet, H., Colin, C., Thierens, M., Latruwe, K., Van Rooij, D., Foubert, A., Frank, N., Blamart, D., Huvenne, V.A.I., Swennen, R., Vanhaecke, F., & Henriet, J.-P.

(2011), The importance of the terrigenous fraction within a cold-water coral mound: A case study. Marine Geology, 282, 13-25.

Pirlet H., LM Wehrmann, B Brunner, N Frank, J Dewanckele, D Van Rooij, A. Foubert, R. Swennen, L. Naudts, M. Boone, V. Cnudde, J.,ÄêP. Henriet (2009) Diagenetic formation of gypsum and dolomite in a cold,Äêwater coral mound in the Porcupine Seabight, off Ireland. Sedimentology 57 (3), 786-805

Pollard, R. T., J. F. Read, and N. P. Holliday (2004) Pollard Water masses and circulation pathways through the Iceland Basin during Vivaldi 1996. Journal of Geophysical Research, 109, C04004

Pons-Branchu, E., Douville, E., Roy-Barman, M., Dumont, E., Branchu, P., Thil, F., Frank, N., Bordier, L., & Borst, W. (2014), A geochemical perspective on Parisian urban history based on U-Th dating, laminae counting and yttrium and REE concentrations of recent carbonates in underground aqueducts. Quat. Geochronol., 24, 44-53.

Pons-Branchu, E., Hillaire-Marcel, C., Ghaleb, B., Deschamps, P., & Sinclair, D. (2005), Early diagenesis impact on precise U-series dating of Deep-Sea corals. Example of a 100-200 years old *Lophelia pertusa* sample from NE Atlantic. Geochimica et Cosmochimica Acta, 69 (20), 4865-4879.

Prins, M. A., L. M. Bouwer, C. J. Beets, S. R. Troelstra, G. J. Weltje, R. W. Kruk, A. Kuijpers, Vroon, P. Z., (2002), Ocean circulation and iceberg discharge in the glacial North Atlantic: Inferences from unmixing of sediment size distributions, Geology, 30(6), 555-558.

Raddatz, J., Liebetrau, V., Trotter, J., Rüggeberg, A., Flogel, S., Dullo, W.,ÄêC., Eisenhauer, A., Voigt, S., and McCulloch, M. (2016), Environmental constraints on Holocene cold-water coral reef growth off Norway: Insights from a multiproxy approach, Paleoceanography, 31, 1350-1367.

Raddatz, J., Rüggeberg, A., Liebetrau, V., Foubert, A., Hathorne, E.C., Fietzke, J., Eisenhauer, A., & Dullo, W.-C. (2014), Environmental boundary conditions of cold-water coral mound growth over the last 3 million years in the Porcupine Seabight, Northeast Atlantic. Deep Sea Research Part II: Topical Studies in Oceanography, 99, 227-236.

Robinson, L. F., Adkins, J. F., Frank, N., Gagnon, A. C., Prouty, N. G., Roark, E. B. & van de Flierdt, T. (2014) The geochemistry of deep-sea coral skeletons: A review of vital effects and applications for palaeoceanography. Deep Sea Research Part II: Topical Studies in Oceanography. 105, p.118-118 (vol 99, pg 184, 2014).

Roberts, D. Long, J.B. Wilson, P.B. Mortensen, J.D. Gage, (2003) The cold-water coral *Lophelia pertusa* (Scleractinia) and enigmatic seabed mounds along the north-east Atlantic margin: are they related? Marine Pollution Bulletin 46 (2003) 7-20

Roberts, J.M., Wheeler, A., Freiwald, A., Cairns, S.D., 2009. Cold-Water Corals: The Biology and Geology of Deep-Sea Coral Habitats. Cambridge University Press, Cambridge.

Roberts, J.M., Wheeler, A., Freiwald, A., 2006. Reefs of the deep: the biology and geology of cold-water coral ecosystems. Science 312, 543-547.

Roberts, J.M., Davies, A.J., Henry, L.A., Dodds, L.A., Duineveld, G.C.A., Lavaleye, M.S.S., Maier, C., van Soest, R.W.M., Bergman, M.J.N., Huhnerbach, V., Huvenne, V.A.I., Sinclair, D. J., Watmough, T., Long, D., Green, S.L., & van Haren., H. (2009), Mingulay reef complex: an interdisciplinary study of cold-water coral habitat, hydrography and biodiversity. Marine ecology progress series, 397, 139-151.

Rüggeberg A, Dullo C, Dorschel B, Hebbeln D (2007) Environmental changes and growth history of Propeller Mound, Porcupine Seabight: evidence from benthic foraminiferal assemblages. Int J Earth Sci 96:57-72.

Sánchez, F., González-Pola, C., Druet, M., García-Alegre, A., Acosta, J., Cristobo, J., Parra, S., Ríos, P., Altuna, Á., Gómez-Ballesteros, M., Muñoz-Recio, A., Rivera, J., & del Río, G.D. (2014), Habitat characterization of deep-water coral reefs in La Gaviera Canyon (Avilés Canyon System, Cantabrian Sea). Deep Sea Research Part II: Topical Studies in Oceanography, 106, 118-140.

Sarnthein, M., et al. (1995), Variations in Atlantic surface ocean paleoceanography, 50° - 80°N: A time-slice record of the last 30,000 years, Paleoceanography, 10(6), 1063-1094, doi:10.1029/95PA01453.

Schmidt, F., Schmidt, A., Treguier, E., Guiheneuf, M., Moussaoui, S., Dobigeon, N., 2010. Implementation Strategies for Hyperspectral Unmixing Using Bayesian

Source Separation, IEEE Transactions on Geoscience and Remote Sensing, 48, 4003-4013.

Schröder-Ritzau, A., Freiwald, A., & Mangini, A. (2005), U/Th-dating of deep-water corals from the eastern North Atlantic and the western Mediterranean Sea. In: Freiwald A, Roberts J.M. (eds) Cold-Water Corals and Ecosystems, Springer-Verlag, Berlin-Heidelberg, pp 1151-1169.

Simpson, John J. & E. Hill, A. (1986). The Scottish Coastal Current. 295-308. 10.1007/978-3-642-70886-2_21.

Somoza, L., Ercilla, G., Urgorri, V., Le√≥n, R., Medialdea, T., Paredes, M., Gonzalez, F.J., & Nombela, M.A. (2014), Detection and mapping of cold-water coral mounds and living *Lophelia* reefs in the Galicia Bank, Atlantic NW Iberia margin. Marine Geology, 349, 73-90.

Thierens, M., Pirlet, H., Colin, C., Latruwe, K., Vanhaecke, F., Stuut, J.-B., Titschack, J., Huvenne, V.A.I., Dorschel, B., Wheeler, A.J., & Henriet, J.-P. (2012), Evidence for an ice-rafting British-Irish ice sheet since the earliest Pleistocene (2.6 million years ago)): early mid-latitudinal glaciation around the North Atlantic Ocean. Quaternary Science Reviews, 44, 229-240.

Thierens, M., Browning, E., Pirlet, H., Loutre, M.-F., Dorschel, B., Huvenne, V.A.I., Titschack, J., Colin, C., Wheeler, A.J. (2013). Coral-water carbonate mounds as unique palaeo-archives: the Plio-Pleistocene Challenger Mound record (NE Atlantic), Quaternary Science Reviews, 73, 14-30.

Thornalley, D.J., Elderfield, H., & McCave, N. (2009), Holocene oscillations in temperature and salinity of the surface subpolar North Atlantic. Nature, 457, 711-714.

Thornalley, D.J.R., Blaschek, M., Davies, F.J., Praetorius, S., Oppo, D.W., McManus, J.F., Hall, I.R., Kleiven, H., Renssen, H., McCave, I.N., (2013), Long-term variations in Iceland-Scotland overflow strength during the Holocene, Clim. Past, 9, 2073-2084.

Teichert C., (1958) Cold- and Deep-Water Coral Banks AAPG Bulletin 42(5):1064-1082

van der Land, C., Eisele, M., Mienis, F., de Haas, H., Hebbeln, D., Reijmer, J.J.G., & van Weering., T.C.E. (2014) Carbonate mound development in contrasting settings on the Irish margin. Deep-Sea Research Part I, Topical Studies in Oceanography, 99, 297-306.

Veron JEN (1993) Corals of Australia and the Indo-Pacific. University of Hawaii Press, Honolulu, HI

Victorero, L., Blamart, D., Pons-Branchu, E., Mavrogordato, M.N., Huvenne, V.A.I. (2016) Reconstruction of the formation history of the Darwin Mounds, N Rockall Trough: How the dynamics of a sandy contourite affected cold-water coral growth. Marine Geology, 378, 186-195.

Waelbroeck C.; Duplessy, J-C.; Michel, E.; Labeyrie, L.; Paillard, D. Duprat, J. (2001) The timing of the last deglaciation in North Atlantic climate records, Nature volume 412, pages 724-727

Waelbroeck C, et al. (2002) Sea-level and deep water temperature changes derived from benthic foraminifera isotopic records. Quat Sci Rev 21:295-305

Weltje, G.J., 1997. End-member modeling of compositional data: numerical-statistical algorithms for solving the explicit mixing problem, Mathematical Geology, 29, 503-549.

White, M. & Bowyer, P. The shelf-edge current north-west of Ireland Annales Geophysicae (1997) 15: 1076.

White M (2007) The hydrography of the Porcupine Bank and Sea Bight and associated carbonate mounds. Int J Earth Sci 96:1-9

Wienberg C., Hebbeln D., Fink H.G., Mienis F, Dorschel B., Vertino A., López-Correa M., Freiwald A. (2009). Scleractinian cold-water corals in the Gulf of Cádiz-First clues about their spatial and temporal distribution. Deep Sea Research Part I Oceanographic Research Papers. 56. 1873-1893. 10.1016/j.dsr.2009.05.016.

Wienberg C., Hebbeln D., Fink H.G., Mienis F, Dorschel B., Vertino A., López - Correa M., Freiwald A. (2010). Glacial cold-water coral growth in the Gulf of Cádiz: Implications of increased palaeo-productivity. Earth and Planetary Science Letters. 298. 405-416. 10.1016/j.epsl.2010.08.017.

Windom, H.L. (1976) Lithogenous material in marine sediments. In: Riley J.P., Chester R., Eds., Chemical Oceanography. Academic Press, New York, London, 5:103-135.

Wyville-Thomson, C., 1874. In: The Depths of the Sea. MacMillan and Co., London, p. 527.

Ziska H.; Varming, T. (2008) Palaeogene evolution of the Ymir and Wyville Thomson ridges, European North Atlantic margin Geological Society, London, Special Publications, 306, 153-168, 7 in JOHNSON, H., DORE, A. G., GATLIFF, R. W., HOLDSWORTH, R., LUNDIN, E. R. &RITCHIE, J. D. (eds) The Nature and Origin of Compression in Passive Margins. Geological Society, London, Special Publications, 306, 153-168

Figures and Tables

Figure 1 : Map of the study area showing the location of vibrocore +59-07/923VE investigated in this study (yellow star). Other cores discussed in this paper are also reported in the insert (open dots) : (1) MD01-2454G; (2) Na-87-22; (3) +56-08/929VE and +56-08/930VE. Arrows represent the main subsurface oceanographic currents. NAC: North Atlantic Current; SEC: Shelf Edge Current; SCC : Scottish Coastal Current as shown in (Inall et al., 2009). The position of the maximum extent on the British Ice Sheet is show dashed line modified from Clarck et al., (2010).

Figure 2 : Vibrocore 59-07/293VE detailed plot of U/Th and ^{14}C dates from 0-300 cm. U/Th *L. pertusa* dates (empty circles) and ^{14}C *L. pertusa* dates (full circles) and ^{14}C benthic foraminifera *C. refulgen* dates (full squares). Sedimentation rates are estimated using ^{14}C data are (indicated on the right side of the plot (black)) and U/Th data are indicated (on the left side of the plot (bold red). Mean sedimentation rates are estimated from 160-290 cm (brown full and empty circles) and from 0-60 cm (red full and empty circles). Significant differences of sedimentation rates are observed between the U/Th and ^{14}C ages are observed in the section 160-290 cm (34.8 cm/ka for U/Th data and 70.9 cm/ka for the ^{14}C data). Similar sedimentation rates are observed in the section 0-60 cm (9.1 cm/ka for U/Th and 6.9 cm/ka for ^{14}C data).

Figure 3 : Vibrocore 59-07/293VE Grain-size data: A- EM1, EM2 and EM3 size distributions; B - Vibrocore 59-07/293VE grain-size data versus depth and C - Mean grain size versus depth.

Figure 4: Vibrocore 59-07/293VE all data versus depth. The grey band highlights the reworked zone between depth 60-160 cm with absence of well- preserved large fragments of *L pertusa* samples. From top to bottom: A: grain-size data. B: clay mineralogy. C: δ^{18}O profile of *G. bulloides* (left axis) and abundance of coral fragments > 2 cm (right axis). D: Age depth distribution in cal ka BP (U/Th (black diamonds) and ^{14}C dates for *L. pertusa* (red squares) *C. refulgens* (blue circles)

and marine bivalves (green triangles)) and right axis number of coral fragments > 2 cm. The dashed lines highlight the transitions at 300 and 400 cm discussed herein.

Figure 5 : Vibrocore 59-07/293VE all data versus age. The blue shaded area highlights the glacial age deposits > 13 cal ka BP with average mean sedimentation rate of 2 cm/ka (the age scale is compressed for easier viewing). The red shaded area highlights the end of the deglacial/early Holocene with average mean sedimentation rates of 35-8 cm/ka and the yellow shaded area highlights the period from 9 cal ka BP-modern period when abundant CWC are found and mean sedimentation is the highest: 30-40 cm/ka. From top to bottom: A: grain grain-size data. B: clay mineralogy. C: $\delta^{18}O$ and $\delta^{13}C$ profiles of *G. bulloides* of core 59-07/293VE (green and red) and Na87-22 (blue and grey). D: Age depth relationship for the stratigraphic age model (blue line) and the distribution of U/Th (black open circles) and ^{14}C dates for *L. pertusa* (full brown circles) *C. refulgens* (red squares) and marine bivalves (green triangles). The tie points for the stratigraphic age model with (blue squares). Mean sediment rates are indicated for the stratigraphic age model. The glacial section (13-50ka) of this diagram has been compressed in order to facilitate viewing of the transitions at 9 and 13 cal ka BP.

Table 1 : Calibrated AMS ^{14}C age. ^{14}C ages were converted into calendar years (cal. yr BP, BP = AD 1950) by using the Marine13 calibration data set and the CALIB 7.04 program (Stuiver et al., 2005; Reimer et al., 2013). A mean reservoir effect of ~400 years has been used.

Table 2 : $^{230}Th/^{234}U$ ages for CWC: U and Th content, uranium isotopic initial ratio (expressed as $\delta^{234}Uo = ([^{234}U/^{238}U]_0 - 1) \times 1000$) and corrected ages for detrital fraction using ($^{230}Th/^{232}Th$) = 10 ± 4. Ages are expressed as ka before 1950.

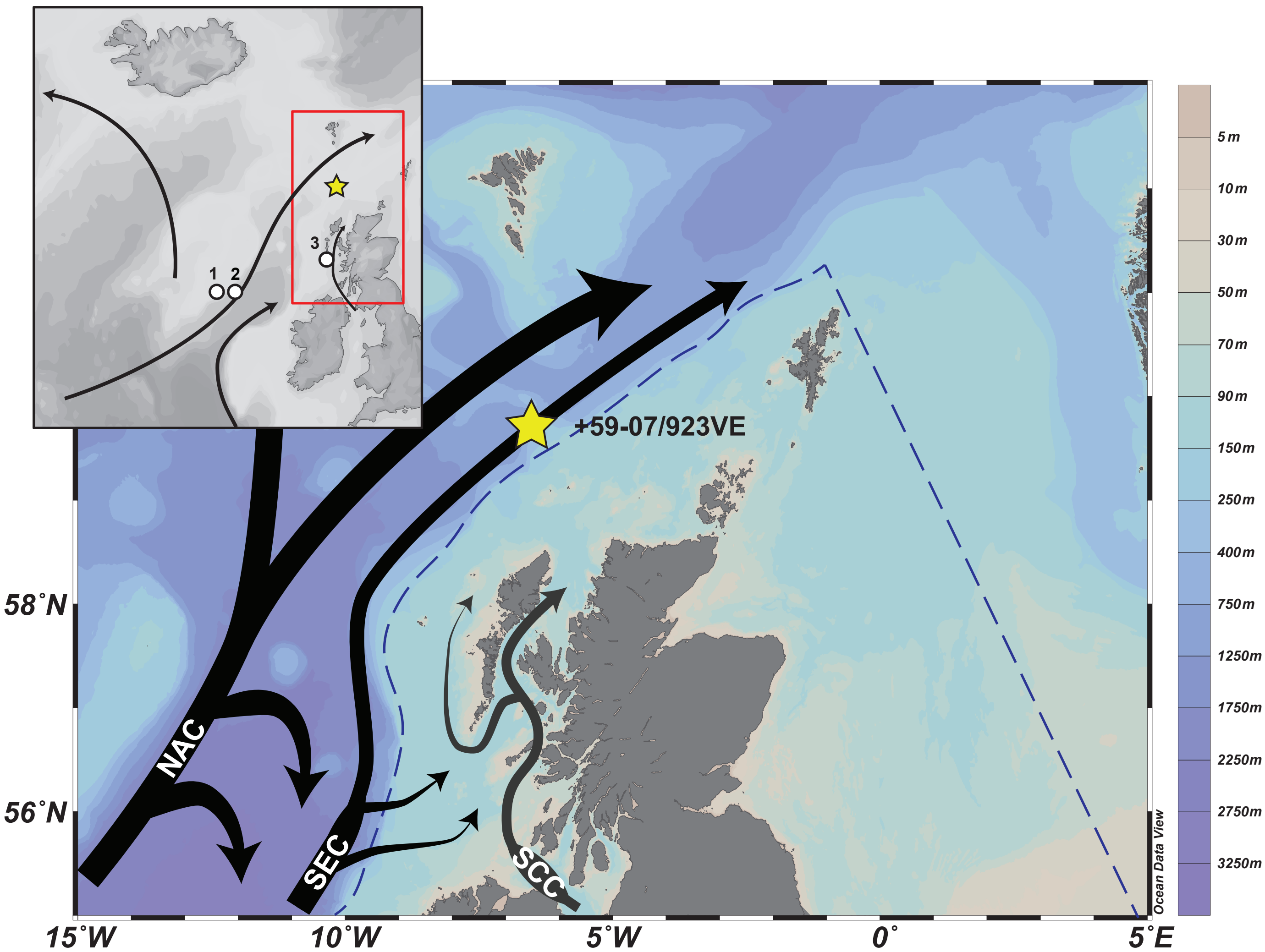

1
2
3
+59-07/923VE
NAC
SEC
SCC
58˚N
56˚N
15˚W
10˚W
5˚W
0˚
5˚E
5 m
10 m
30 m
50 m
70 m
90 m
150 m
250 m
400 m
750 m
1250 m
1750 m
2250 m
2750 m
3250 m
Ocean Data View

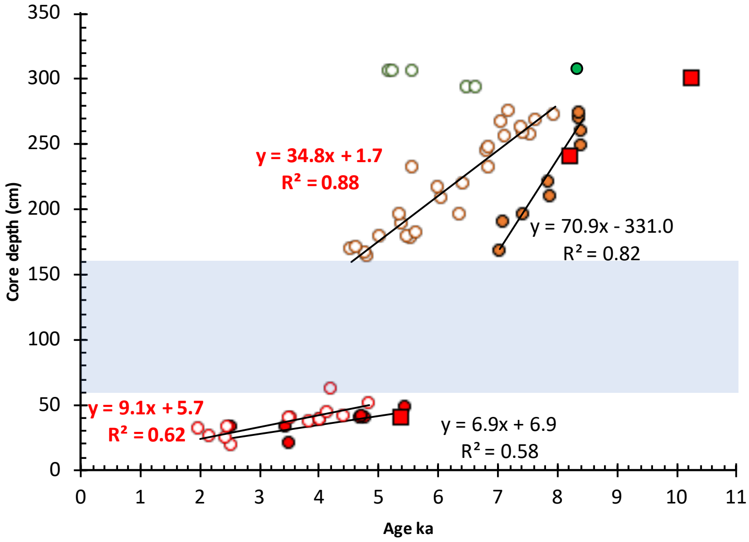

Core depth (cm)
Age ka
350
300
250
200
150
100
50
0
0
1
2
3
4
5
6
7
8
9
10
11
y = 34.8x + 1.7
R² = 0.88
y = 70.9x - 331.0
R² = 0.82
y = 9.1x + 5.7
R² = 0.62
y = 6.9x + 6.9
R² = 0.58

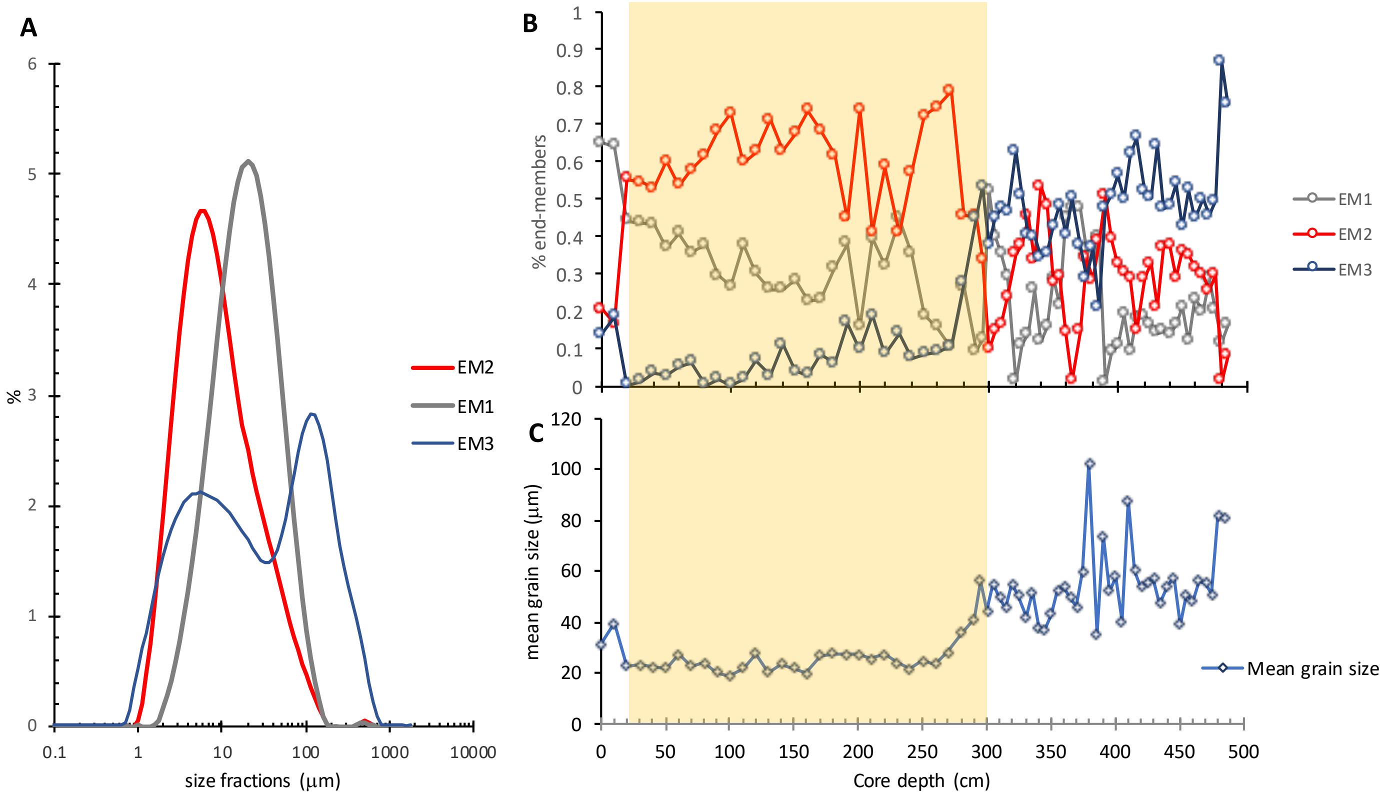
A
%
size fractions (µm)
EM2
EM1
EM3
B
% end-members
EM1
EM2
EM3
C
mean grain size (µm)
Mean grain size
Core depth (cm)

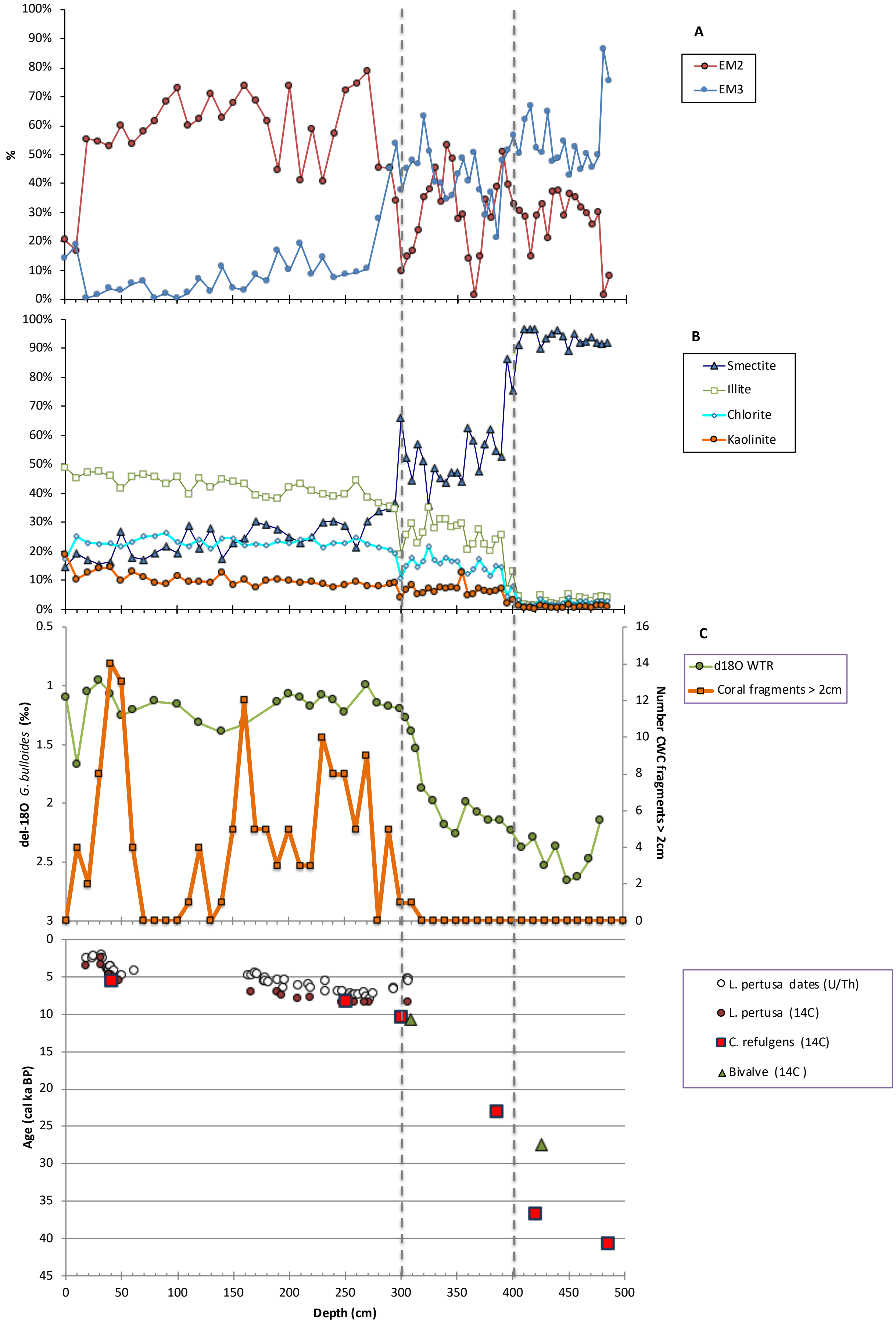

A
EM2
EM3
%
B
Smectite
Illite
Chlorite
Kaolinite
C
d18O WTR
Coral fragments > 2cm
del-18O G. bulloides (‰)
Number CWC fragments > 2cm
L. pertusa dates (U/Th)
L. pertusa (14C)
C. refulgens (14C)
Bivalve (14C)
Age (cal ka BP)
Depth (cm)

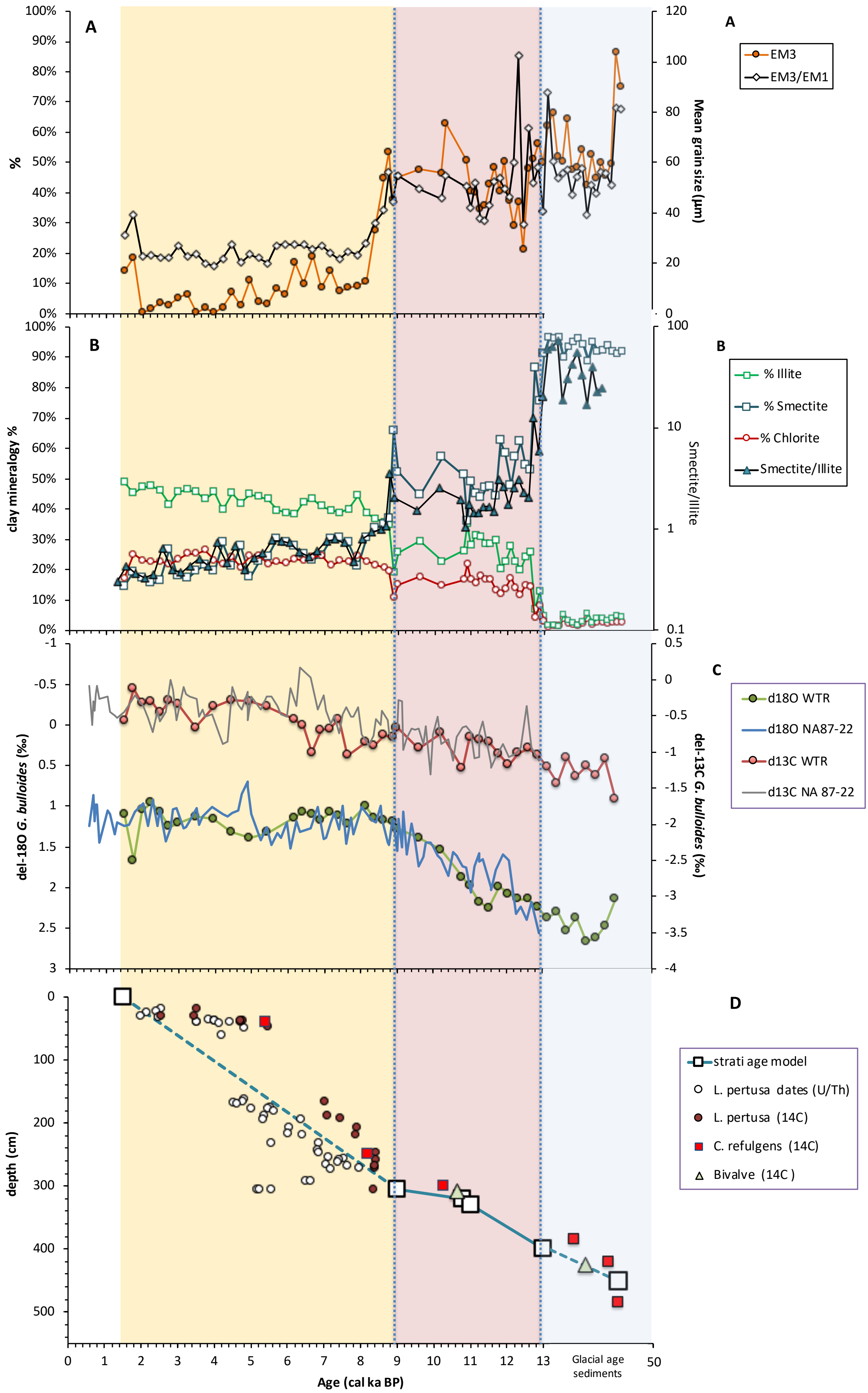
A
B
C
D
EM3
EM3/EM1
%
Mean grain size (µm)
% Illite
% Smectite
% Chlorite
Smectite/Illite
clay mineralogy %
d18O WTR
d18O NA87-22
d13C WTR
d13C NA 87-22
del-18O G. bulloides (‰)
del-13C G. bulloides (‰)
strati age model
L. pertusa dates (U/Th)
L. pertusa (14C)
C. refulgens (14C)
Bivalve (14C)
depth (cm)
Glacial age sediments
Age (cal ka BP)

N° GifA / SacA	Depth (cm)	species	Age BP	Err âge BP (1σ)	Cal years BP Median Probability	2 σ range cal years BP	
14366 / 40200	19	*L pertusa*	3625	35	**3522**	cal BP 3424 - 3627	
14367 / 40201	31.5	*L pertusa*	2800	30	**2557**	cal BP 2423 - 2682	
15305 / 42891	32	*L pertusa*	3575	30	**3465**	cal BP 3378 - 3554	*
14368 /40202	38.5	*L pertusa*	4580	30	**4805**	cal BP 4689 - 4863	
15306 / 42892	39	*L pertusa*	4520	30	**4730**	cal BP 4612 - 4817	*
14369 / 40203	41	*L pertusa*	4525	30	**4736**	cal BP 4618 - 4820	
15308 / 42894	48	*L pertusa*	5100	30	**5470**	cal BP 5332 - 5338	*
14371 / 40205	166.5	*L pertusa*	6530	40	**7047**	cal BP 6929 - 7155	
14372 / 40206	189	*L pertusa*	6590	35	**7115**	cal BP 6999 - 7217	
15309 / 42895	194	*L pertusa*	6945	30	**7450**	cal BP 7394 - 7524	*
14373 / 40207	208	*L pertusa*	7450	40	**7911**	cal BP 7819 - 7995	
14374 / 40208	219	*L pertusa*	7415	40	**7880**	cal BP 7819 - 7995	
14376 / 40210	247	*L pertusa*	7985	50	**8443**	cal BP 8346 - 8552	
14377 / 40211	258.5	*L pertusa*	7990	45	**8447**	cal BP 8357 - 8548	
15310 /42896	268	*L pertusa*	7945	30	**8400**	cal BP 8335 - 8485	*
14378 / 40212	272	*L pertusa*	7960	40	**8417**	cal BP 8357 - 8548	
14379 / 40213	306	*L pertusa*	7920	45	**8381**	cal BP 8357 - 8548	
15312 / 42898	40	*C. refulgens*	5060	30	**5410**	cal BP 4612 - 4817	*
15313 / 42899	250	*C. refulgens*	7745	30	**8220**	cal BP 8144 - 8309	*
15314 / 42900	300	*C. refulgens*	9440	30	**10271**	cal BP 10196 - 10383	*
15315 / 42901	385	*C. refulgens*	19430	70	**22905**	cal BP 22619 - 23160	*
15317 / 42903	420	*C. refulgens*	33080	270	**36643**	cal BP 35998 - 37633	*
15318 / 42904	485	*C. refulgens*	36430	390	**40655**	cal BP 39804 - 41461	*
15319 / 42905	308	*V. casima*	9750	35	10650	cal BP 10196 - 10383	*
15320 / 42906	425	*Venus sp.*	23490	100	**27396**	cal BP 27171 - 27603	*
15321 / 42907	480	*Venus sp.*	48800	1700	**>50000**		

Lab-code	sample-label	mean depth (cm)	[^{238}U] (ppm)		[^{232}Th] (ppm)		$\delta^{234}U_m$ (‰)		^{230}Th/^{238}U		^{230}Th/^{232}Th		δ^{234}U(0) (‰)		**age (kyr)**		**age (kyr) Cor BP**	
5426	18-20	19	4.238	0.004	0.1407	0.0004	145.6	0.7	0.0273	0.0001	2639.4	13.3	146.6	0.7	2.63	0.02	2.555	0.019
5428	23-25	24	3.775	0.004	0.2042	0.0005	145.9	0.7	0.0261	0.0002	1551.6	9.9	146.9	0.7	2.52	0.02	2.437	0.024
5427	21-29	25	3.552	0.004	0.1099	0.0003	145.9	0.7	0.0233	0.0001	2414.1	14.4	146.8	0.8	2.24	0.01	2.166	0.019
5268	29-34	31.5	4.189	0.007	0.1067	0.0003	145.9	1.0	0.0216	0.0001	2639.6	13.2	146.8	1.0	2.08	0.01	2.004	0.015
5429	32-33	32.5	4.432	0.007	0.2132	0.0004	146.1	0.8	0.0266	0.0003	1777.7	18.8	147.2	0.8	2.56	0.03	2.482	0.035
5592	36-38	37	3.899	0.007	0.1459	0.0006	145.2	1.2	0.0404	0.0002	3408.1	18.6	146.9	1.2	3.92	0.03	3.846	0.030
5703	37-39	38	3.949	0.012	0.1597	0.0008	145.6	1.3	0.0423	0.0003	3319.4	22.1	147.3	1.3	4.11	0.03	4.033	0.037
5267	37-40	38.5	3.517	0.007	0.1353	0.0006	145.4	0.8	0.0422	0.0002	3427.3	15.3	147.1	0.8	4.10	0.02	4.021	0.026
5704bis	39-41	40	4.147	0.015	0.1684	0.0008	143.3	1.0	0.0372	0.0002	2896.5	17.1	144.8	1.1	3.61	0.02	3.533	0.030
5704	39-41	40	4.125	0.006	0.1746	0.0010	148.5	0.6	0.0373	0.0002	2832.5	15.4	150.0	0.6	3.60	0.02	3.523	0.027
5266	40-42	41	3.552	0.004	0.1199	0.0003	146.4	0.8	0.0465	0.0002	4400.0	19.0	148.3	0.8	4.52	0.02	4.445	0.027
5593	40-46	43	3.783	0.005	0.3153	0.0012	144.9	0.6	0.0437	0.0002	1657.9	8.7	146.6	0.6	4.25	0.02	4.158	0.035
5265	48-52	50	3.181	0.007	0.1936	0.0008	145.5	0.6	0.0505	0.0002	2608.9	8.8	147.6	0.6	4.92	0.02	4.841	0.027
5594	60-63	61.5	3.406	0.007	0.1809	0.0008	144.8	0.8	0.0441	0.0002	2627.6	14.4	146.6	0.8	4.29	0.03	4.207	0.034
5264	161-166	163.5	4.123	0.004	0.2157	0.0007	145.4	0.7	0.0503	0.0002	3014.5	11.6	147.4	0.7	4.90	0.02	4.820	0.028
5263	165-168	166.5	3.838	0.006	0.3510	0.0011	145.1	0.6	0.0502	0.0002	1712.7	6.7	147.1	0.6	4.89	0.02	4.801	0.033
5705	168-170	169	3.907	0.006	0.2673	0.0008	144.2	0.7	0.0475	0.0002	2230.8	8.0	146.1	0.7	4.63	0.02	4.542	0.028
5595	170-172	171	4.191	0.008	0.3109	0.0028	144.3	0.9	0.0486	0.0005	2054.7	23.1	146.3	0.9	4.74	0.06	4.649	0.067
5262	175-179	177	3.465	0.004	0.2475	0.0009	145.9	0.6	0.0576	0.0003	2530.2	11.3	148.2	0.6	5.63	0.03	5.542	0.038
5707	178-179	178.5	3.502	0.005	0.3701	0.0011	145.3	0.6	0.0526	0.0002	1605.6	5.3	147.4	0.6	5.13	0.02	5.039	0.033
5706	175-182	178.5	3.544	0.004	0.1933	0.0002	146.1	0.9	0.0571	0.0001	3198.8	6.3	148.4	0.9	5.58	0.02	5.497	0.023
5596	180-182	181	3.349	0.008	0.3901	0.0017	143.8	0.9	0.0587	0.0003	1582.8	7.4	146.2	0.9	5.75	0.03	5.645	0.046
5261	187-191	189	3.669	0.007	0.9898	0.0038	143.1	0.7	0.0566	0.0003	658.1	3.7	145.3	0.7	5.54	0.04	5.396	0.068
5708	194-196	195	4.019	0.009	0.2034	0.0029	145.3	1.1	0.0658	0.0009	4135.4	59.9	147.9	1.1	6.45	0.10	6.375	0.108
5260	194-198	196	4.120	0.008	0.1098	0.0005	143.9	0.8	0.0556	0.0003	6527.3	31.3	146.2	0.8	5.44	0.03	5.364	0.034
5259	206-210	208	4.127	0.008	0.2235	0.0008	144.0	0.8	0.0628	0.0002	3631.1	13.3	146.5	0.8	6.16	0.03	6.075	0.034
5709	215-219	217	4.216	0.008	0.2455	0.0009	145.6	0.8	0.0623	0.0003	3405.6	14.9	148.1	0.8	6.10	0.03	6.024	0.039
5258	217-221	219	4.264	0.010	0.3412	0.0015	145.1	0.8	0.0664	0.0003	2596.8	13.1	147.8	0.8	6.52	0.04	6.427	0.048
5257	231-233	232	4.509	0.018	0.3317	0.0013	144.5	1.0	0.0579	0.0002	2462.5	8.6	146.8	1.0	5.66	0.03	5.578	0.035
5710	230-234	232	3.563	0.008	0.1546	0.0024	142.0	0.8	0.0705	0.0004	5160.8	28.3	144.9	0.9	6.95	0.04	6.876	0.050

5597	241-246	243.5	3.620	0.018	0.1612	0.0009	142.6	1.3	0.0701	0.0005	4929.1	34.0	145.4	1.4	6.91	0.06	6.829	0.063
5256	245-249	247	3.684	0.005	0.2832	0.0014	146.1	0.7	0.0708	0.0003	2881.8	12.2	149.0	0.7	6.96	0.03	6.872	0.045
5711	253-257	255	3.727	0.006	0.5141	0.0016	146.9	1.1	0.0737	0.0003	1715.4	7.4	149.9	1.1	7.24	0.04	7.134	0.055
5712	255-258	256.5	3.857	0.011	0.3328	0.0013	143.6	1.2	0.0775	0.0003	2846.4	12.7	146.8	1.2	7.65	0.04	7.562	0.054
5255	257-260	258.5	3.310	0.005	0.1561	0.0006	144.3	0.7	0.0761	0.0003	5050.5	20.8	147.4	0.7	7.51	0.04	7.429	0.043
5713	260-264	262	3.298	0.009	0.2888	0.0020	145.6	1.4	0.0761	0.0006	2755.8	21.0	148.7	1.4	7.50	0.07	7.405	0.079
5714	265-268	266.5	3.404	0.009	0.3629	0.0013	142.8	1.2	0.0726	0.0004	2162.2	11.7	145.7	1.2	7.16	0.05	7.066	0.061
5598	267-270	268.5	3.942	0.013	0.4034	0.0017	142.9	1.2	0.0785	0.0003	2413.1	10.7	146.1	1.2	7.76	0.04	7.660	0.056
5254	269-275	272	3.490	0.005	0.2753	0.0010	144.5	0.6	0.0815	0.0003	3234.3	12.5	147.8	0.6	8.05	0.04	7.966	0.046
5253	272-278	275	4.021	0.028	0.3347	0.0029	144.7	0.7	0.0741	0.0002	2739.3	6.9	147.7	0.7	7.30	0.02	7.209	0.034
5252	291-295	293	3.670	0.008	0.3228	0.0005	144.5	1.1	0.0672	0.0002	2354.6	8.3	147.2	1.1	6.60	0.02	6.514	0.034
5430	291-295	293	3.820	0.006	0.1289	0.0003	144.2	0.9	0.0685	0.0003	6536.4	25.0	146.9	0.9	6.74	0.03	6.662	0.036
5431	305-306	305.5	4.482	0.006	0.2389	0.0007	144.6	0.8	0.0541	0.0003	3248.9	15.5	146.8	0.8	5.28	0.03	5.204	0.036
5432	305-307 b	306	4.166	0.006	0.1602	0.0007	144.6	1.0	0.0545	0.0003	4539.4	22.1	146.8	1.0	5.33	0.03	5.250	0.036
5251	305-307	306	4.052	0.008	0.3649	0.0005	145.2	1.0	0.0582	0.0001	1989.6	4.5	147.5	1.0	5.69	0.02	5.594	0.029